

# Structured Prototype-Guided Adaptation for EEG Foundation Models

Jingying Ma<sup>1\*</sup>, Feng Wu<sup>1\*</sup>, Yucheng Xing<sup>1,3</sup>, Qika Lin<sup>1</sup>, Tianyu Liu<sup>1,3</sup>,  
 Chenyu Liu<sup>4†</sup>, Ziyu Jia<sup>5,6†</sup>, Mengling Feng<sup>1,2</sup>

<sup>1</sup>Saw Swee Hock School of Public Health, National University of Singapore, Singapore

<sup>2</sup>Institute of Data Science, National University of Singapore, Singapore

<sup>3</sup>Guangzhou Research Translation and Innovation Institute,  
 National University of Singapore, Guangzhou, China

<sup>4</sup>College of Computing and Data Science, Nanyang Technological University, Singapore

<sup>5</sup>Beijing Key Laboratory of Brainnetome and Brain-Computer Interface,  
 Institute of Automation, Chinese Academy of Sciences, Beijing, China

<sup>6</sup>Brainnetome Center, Institute of Automation, Chinese Academy of Sciences, Beijing, China

## Abstract

Electroencephalography (EEG) foundation models (EFMs) have achieved strong performance under full fine-tuning but exhibit poor generalization when subject-level supervision is limited, a common constraint in real-world clinical settings. We show that this failure stems not merely from limited supervision, but from *a structural mismatch between noisy, limited supervision and the highly plastic parameter space of EFMs*. To address this challenge, we propose *SCOPE*, a Structured COnfidence-aware Prototype-guided adaptation framework for EFM fine-tuning. *SCOPE* follows a two-stage pipeline. In the first stage, we construct reliable external supervision by learning geometry-regularized task priors, constructing balanced class-level prototypes over the resulting embeddings, and producing confidence-aware pseudo-labels from their agreement to filter unreliable signals on unlabeled data. In the second stage, we introduce *ProAdapter*, which adapts frozen EEG foundation models via a lightweight adapter conditioned on the structured prototypes. Experiments across three EEG tasks and five foundation model backbones demonstrate that *SCOPE* consistently achieves strong performance and efficiency under label-limited cross-subject settings.

## 1 Introduction

Electroencephalography (EEG) is widely used to characterize brain states across clinical contexts [Pellinen et al., 2024, Mushtaq et al., 2024], enabling sleep staging [Ye et al., 2020], affective assessment [Sun et al., 2024], and noninvasive brain-computer interfaces [Ding et al., 2025]. Recent research has increasingly shifted from task-specific models [Liu et al., 2024, Ma et al., 2025a] toward EEG foundation models (EFMs), which leverage large-scale pretraining to learn transferable representations across tasks and datasets [Zhou et al., 2025b, Wang et al., 2026a, Huang et al., 2026]. In experimental settings, EFMs achieve strong performance via full fine-tuning, making it the dominant adaptation strategy in current EFM research [Zhou et al., 2025c].

Despite strong benchmark performance, *EFMs exhibit clear generalization degradation under full fine-tuning when supervision is limited to a small number of subjects*. As shown in Figure 1(A), training on 30% of subjects produces a substantially larger generalization gap than full supervision. This observation indicates that **full fine-tuning is unreliable for practical EEG deployments**, where supervision is inherently limited [Lea and Jones, 2024]. In practice, reliable labels are obtained at the subject level and require expert annotation, resulting in only a few labeled subjects with substantially more unlabeled recordings [Ma et al., 2025b].

We further observe several anomalous behaviors when fully fine-tuning EFMs under data-limited conditions: **early-stage training instability** (Figure 2(A), left); **high sensitivity to random initialization** (Figure 2(B)); and **overconfident but inaccurate predictions** (Figure 2(C)). Taken together, these observations suggest that the unreliability of full fine-tuning does not simply arise from limited supervision, but rather reflects *a structural mismatch between limited supervision and the large, highly plastic parameter space of EFMs*. Motivated by these

\*Equal Contributions.

†Corresponding Authors: chenyu003@e.ntu.edu.sg, jia.ziyu@outlook.com.

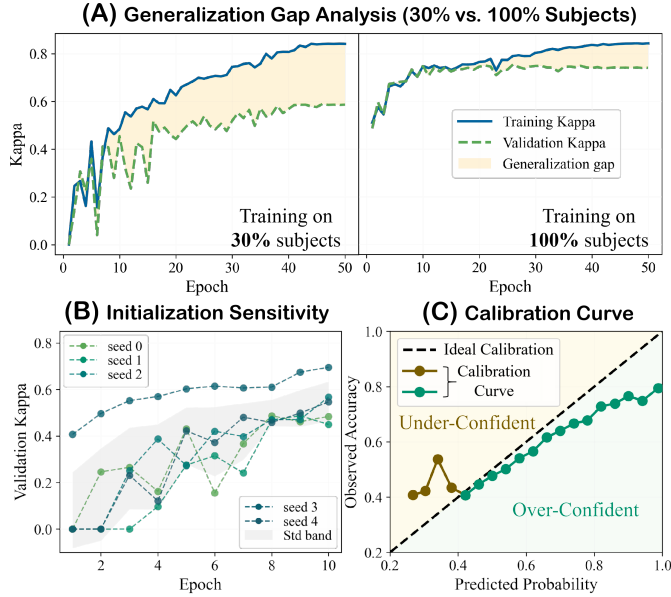


Figure 1: CodeBrain under full fine-tuning on the ISRUC dataset. (A) Training and validation Kappa trajectories, illustrating the generalization gap under 30% versus 100% subjects supervision. (B) Validation Kappa across five random seeds when training with 30% labeled subjects, showing high sensitivity to initialization. (C) Calibration curve on the validation set under 30% subjects supervision, indicating overconfident predictions.

findings, we revisit the problem of adapting EFM under label-limited conditions and identify several key technical challenges.

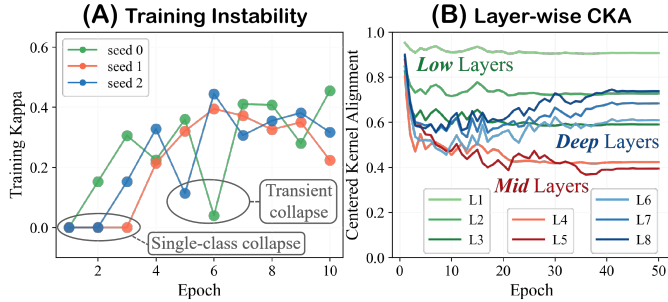


Figure 2: CodeBrain (8-layers EFM backbone) under full fine-tuning on the ISRUC dataset with 30% labeled subjects. (A) Early-stage training dynamics across different random seeds, showing instability and occasional collapse. (B) Layer-wise evolution of parameter space similarity during training, measured by centered kernel alignment (CKA), with low, mid, and deep layers.

**1) EFM fail to provide reliable self-guidance.** Self-training is widely used to leverage unlabeled data under limited supervision in foundation models [Xie et al., 2020, Zhang et al., 2025]. It relies on the assumption that model confidence correlates with prediction accuracy and remains reasonably stable during training [Sohn et al., 2020, Berthelot et al., 2020]. However, as evidenced by instability and overconfidence (Figure 2B and C), EFMs violate these core assumptions, making self-generated supervision potentially misleading and prone to error amplification. More importantly, Figure 1A shows that, under limited-subject supervision, EFMs fit training data well but generalize poorly. This behavior is likely due to strong inter-subject variability of EEG signals, which dominates the representation space when only a few subjects are labeled. In this case, subject-specific patterns overwhelm task-level class structure, encouraging shortcut learning [Geirhos et al., 2020] and rendering label-only adaptation unreliable. Therefore, EFMs require an external source of structured supervision to guide adaptation on unlabeled data.

**2) EFMs are sensitive to estimation bias.** Pseudo-labeling is commonly used to leverage unlabeled data [Zhang et al., 2021a, Wang et al., 2022]. However, properties of EEG data make pseudo-labeling easily biased:

continuous brain states induce ambiguous class boundaries [Zhou et al., 2025a], while class imbalance and intra-class multimodality bias learning toward dominant modes [Berry et al., 2017, Rizve et al., 2021, Guo and Li, 2022]. Unfortunately, EFM are particularly sensitive to such bias, as evidenced by the prediction collapse across random seeds (Figure 2A). Therefore, effective EFM adaptation requires pseudo-labeling that is confidence-aware and robust to imbalance-induced bias.

**3) EFM’s parameter space is vulnerable.** EFM rely on a large pretrained parameter space to encode transferable representations [Zhou et al., 2025b]. Under limited supervision, full fine-tuning leads to large degradation in representation similarity across layers (Figure 2(B)). This reveals that noisy supervision-driven gradients can easily diffuse across layers, overwriting transferable pretrained representations and inducing irreversible optimization drift [Kumar et al., 2022, Ding et al., 2023, Zhang and Wu, 2024]. Therefore, effective adaptation requires persistent constraints that regulate how supervision interacts with the EFM parameter space.

To address the above challenges, we propose *SCOPE*, a Structured CONfidence-aware Prototype-guided adaptation framework for EEG foundation model fine-tuning. *First*, we introduce an *external supervision construction* module to provide structured and confidence-aware guidance for unlabeled data. A lightweight task-prior network, geometrically regularized by an Equiangular Tight Frame (ETF) [Papyan et al., 2020], learns discriminative class-level embeddings. These embeddings are further organized into balanced class prototypes via Sinkhorn-constrained clustering [Sinkhorn and Knopp, 1967, Caron et al., 2020]. Based on the agreement between task-prior predictions and prototype similarity, we derive confidence-aware pseudo-labels that filter uncertain samples and provide stable supervision signals for adaptation. *Second*, we propose a *Prototype-Conditioned Adapter (ProAdapter)*, which freezes backbone parameters and injects lightweight, prototype-conditioned modulation modules into the deeper layers to align updates with the induced class structure. Our main contributions are summarized as follows:

- **External Structured and Confidence-Aware Supervision Construction.** We propose an external module that organizes supervision into structured, class-level prototypes, and incorporates reliability estimation to provide persistent and trustworthy supervision signals for unlabeled data beyond sample-wise labels.
- **Prototype-conditioned Adaptation.** We propose a prototype-conditioned adaptation paradigm that constrains parameter updates by aligning model adaptation with structured external supervision, enabling stable and controlled adaptation of EEG foundation models.
- **Comprehensive Evaluation.** Experiments on 3 EEG tasks and 5 foundation model backbones demonstrate that *SCOPE* consistently achieves strong generalization and efficiency under label-limited conditions.

## 2 Related Work

**Scalp EEG Foundation Models.** Self-supervised pretraining has been widely used to learn transferable EEG representations, including contrastive [Kostas et al., 2021, Karantonis et al., 2025] and reconstruction-based methods [Chien et al., 2022, Mohammadi Foumani et al., 2024]. Much of this work focuses on scalp EEG, enabled by standardized benchmarks [Wang et al., 2025a] and broader data availability [Obeid and Picone, 2016]. Existing EFM mainly adopt sequence modeling backbones, including Transformer-based designs [Yang et al., 2023, Jiang et al., 2024, Wang et al., 2024, Zhou et al., 2025c] and emerging state-space models (SSSMs) [Wang et al., 2025b, Ma et al., 2025c]. Although EFM are powerful, current practice relies on full fine-tuning, which hinders label-efficient adaptation [Lee et al., 2025, Yang et al., 2025, Wang et al., 2026b].

**Parameter-efficient adaptation for foundation models.** Parameter-efficient fine-tuning (PEFT) offers an effective alternative to full fine-tuning in large foundation models, particularly in language and vision models. Prominent PEFT families include weight-space approaches that constrain updates to structured low-dimensional subspaces [Hu et al., 2022, Liu et al., 2022, Zhang et al., 2023], feature-space methods that adapt intermediate representations via conditional modulation [Perez et al., 2018, Mahabadi et al., 2021], and adapter-based techniques that introduce lightweight task-specific modules while keeping the backbone frozen [Houlsby et al., 2019, Karimi Mahabadi et al., 2021]. However, despite their success in language and vision models, PEFT paradigms have only seen limited exploration in EFM [Jeon et al., 2025], and existing studies do not consider label-efficient adaptation under practical deployment.

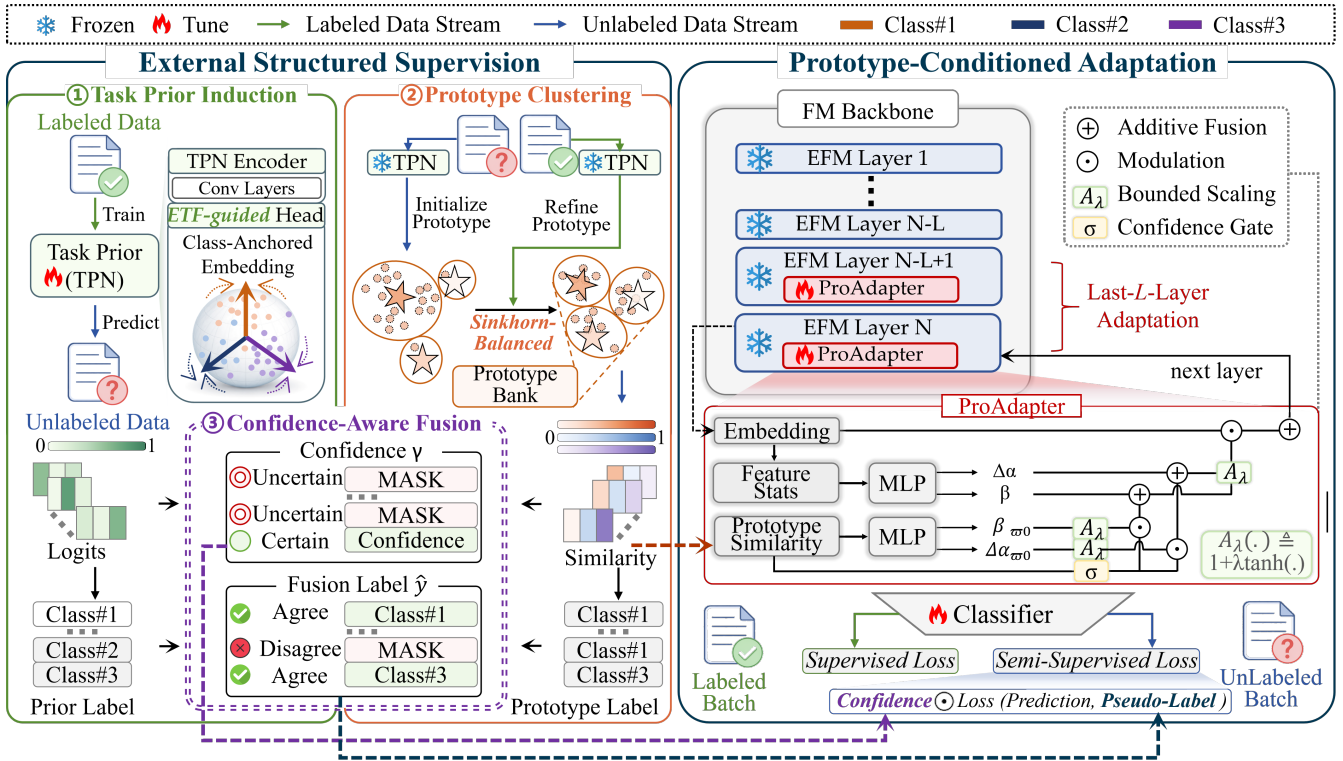


Figure 3: Overview of the two-stage *SCOPE* framework. **Left:** External structured supervision construction progressively induces class-level prototypes and confidence-aware pseudo-labels for unlabeled data. **Right:** A frozen EEG foundation model is adapted via lightweight prototype-conditioned adapters in the last layers, using confidence-weighted supervision for controlled adaptation.

### 3 Methodology

#### 3.1 Problem Setting and Framework Overview

**Label-limited data condition.** Let  $\mathbf{X} \in \mathbb{R}^{C \times T}$  denote an EEG signal with  $C$  channels and length  $T$ . The training data comprise a small labeled set  $\mathcal{D}_l = \{(\mathbf{X}_i, y_i)\}_{i=1}^{N_l}$ , where  $y_i \in \{1, \dots, K\}$  is the label, and a much larger unlabeled set  $\mathcal{D}_u = \{\mathbf{X}_j\}_{j=1}^{N_u}$ . Both sets share the same label space but exhibit distribution shifts due to inter-subject variability.

**Parameter-efficient model adaptation.** We consider a pretrained EEG foundation model (EFM), which maps an EEG sample to a latent representation with frozen backbone parameters. Adaptation is performed by inserting lightweight, trainable modules to modulate intermediate representations.

**Framework Overview.** We study label-limited EFM adaptation, where unlabeled data  $\mathcal{D}_u$  is leveraged to improve downstream performance. Our framework follows a two-stage design: (I) *External structured supervision construction* and (II) *Prototype-conditioned adaptation* (Figure 3).

*Stage I* progressively constructs external supervision for  $\mathcal{D}_u$ . First, a lightweight task-prior network (TPN) is trained on  $\mathcal{D}_l$  with an inter-class geometric regularizer, producing a prior prediction for each unlabeled sample. Second, building on the resulting cluster-friendly embeddings from the TPN, we learn a prototype bank by imposing an intra-class balancing constraint and derive a prototype-based prediction via prototype similarity. The two predictions are then fused to obtain pseudo-labels with calibrated confidence.

*Stage II* adapts the frozen EFM via a lightweight adapter conditioned on prototypes. Training is supervised by fused pseudo-labels with sample-wise confidence weighting.

#### 3.2 External structured supervision construction

To stabilize the adaptation of EFMs under limited labels, we progressively construct external structured supervision for unlabeled data. The constructed supervision encodes inter- and intra-class geometry and prediction reliability,

providing a controllable training signal for subsequent adaptation.

**Task-Prior Induction via Inter-Class Geometry.** We first train a lightweight task-prior network (TPN)  $h_\psi$  on the labeled subset  $\mathcal{D}_l$ , where  $h_\psi$  consists of a feature encoder  $f_\psi$  and a classification head. Given an input EEG sample  $\mathbf{X}_i$ , the encoder produces a task-specific embedding

$$\mathbf{z}_i = f_\psi(\mathbf{X}_i) = \mathcal{H}_{\text{sep}}(\mathcal{H}_{\text{spa}}(\mathcal{H}_{\text{temp}}(\mathbf{X}_i))), \quad (1)$$

where  $\mathcal{H}_{\text{temp}}(\cdot)$ ,  $\mathcal{H}_{\text{spa}}(\cdot)$ , and  $\mathcal{H}_{\text{sep}}(\cdot)$  are a temporal, depthwise spatial, and separable convolution block, respectively (see Appendix J.1 for details).

For multi-class tasks ( $K \geq 3$ ), we impose an Equiangular Tight Frame (ETF)-based geometric regularization to enforce maximal inter-class angular separation, thereby encouraging a cluster-friendly embedding to support subsequent prototype learning with rich intra-class structure.

**Proposition 3.1.** *Let  $\{\tilde{\mathbf{w}}_k\}_{k=1}^K \subset \mathbb{S}^{d-1}$  be the normalized classifier weights. If they satisfy the simplex equiangular tight frame condition  $\tilde{\mathbf{w}}_k^\top \tilde{\mathbf{w}}_{k'} = -\frac{1}{K-1}$ ,  $\forall k \neq k'$ , the minimum pairwise angular separation is maximized.*

Proposition 3.1 provides theoretical motivation for explicit ETF regularization, which yields uniformly separated class-wise embeddings under cross-entropy optimization. Specifically, let  $W = [\mathbf{w}_1, \dots, \mathbf{w}_K] \in \mathbb{R}^{d \times K}$  denote the weight matrix of the linear head. We normalize each class weight as  $\tilde{\mathbf{w}}_k = \mathbf{w}_k / \|\mathbf{w}_k\|_2$  to obtain  $\tilde{W} = [\tilde{\mathbf{w}}_1, \dots, \tilde{\mathbf{w}}_K] \in \mathbb{R}^{d \times K}$  and define an ETF regularizer that penalizes deviations from a simplex equiangular tight frame:

$$\mathcal{L}_{\text{ETF}} = \left\| \tilde{W}^\top \tilde{W} - \left( \frac{K}{K-1} I - \frac{1}{K-1} \mathbf{1} \mathbf{1}^\top \right) \right\|_F^2. \quad (2)$$

where  $\mathbf{1} \mathbf{1}^\top$  denotes an all-ones matrix. The overall training objective of the task-prior network is

$$\mathcal{L}_{\text{TPN}} = \mathcal{L}_{\text{CE}} + \lambda_{\text{ETF}} \mathcal{L}_{\text{ETF}}, \quad (3)$$

where  $\mathcal{L}_{\text{CE}}$  denotes the standard cross-entropy loss and  $\lambda_{\text{ETF}}$  controls the strength of geometric regularization.

After training, the  $h_\psi$  is frozen and applied to the unlabeled set  $\mathcal{D}_u = \{\mathbf{X}_j\}_{j=1}^{N_u}$ . For each unlabeled sample  $\mathbf{X}_j$ , the encoder produces an embedding  $\mathbf{z}_j = f_\psi(\mathbf{X}_j)$ , which is mapped by the linear head to task-prior logits  $\mathbf{s}_j = W^\top \mathbf{z}_j \in \mathbb{R}^K$ . We then derive a prior label by  $\hat{y}_j^{\text{prior}} = \arg \max_k \mathbf{s}_{jk}$ .

**Prototype Clustering via Intra-Class Variability.** Given the inter-class structure induced by the TPN, we further introduce learnable prototypes to capture rich intra-class variability. For each task, we maintain a prototype bank  $\mathcal{P}$  with  $M$  prototypes for each class  $k \in \{1, \dots, K\}$ :

$$\mathcal{P} = \{p_{k,m} \in \mathbb{R}^d \mid m \in \{1, 2, \dots, M\}\}. \quad (4)$$

The prototype bank  $\mathcal{P}$  is initialized via  $k$ -means clustering [Lloyd, 1982] on unlabeled TPN embeddings grouped by predicted prior labels. For a sample  $X_i$  and a prototype  $p_{k,m}$ , we compute their affinity using cosine similarity:

$$s_{i,(k,m)} = \left( \frac{\mathbf{z}_i}{\|\mathbf{z}_i\|_2} \right)^\top \left( \frac{\mathbf{p}_{k,m}}{\|\mathbf{p}_{k,m}\|_2} \right). \quad (5)$$

For class  $k$ , let  $\mathcal{I}_k$  denote the index set of samples assigned to  $k$  with  $B_k = |\mathcal{I}_k|$ . We define the class-wise similarity matrix  $S^{(k)} \in \mathbb{R}^{B_k \times M}$  with entries  $s_{i,m}^{(k)}$ . Accordingly, a soft sample-to-prototype assignment  $Q_{i,m}^{(k)} = \exp(S_{i,m}^{(k)} / \epsilon)$  can be derived, where  $\epsilon$  is a temperature parameter. we optimize  $Q$  to maximize the sample-prototype similarity:

$$\begin{aligned} \max_{Q \in \mathcal{Q}} \quad & \text{Tr}(QS^\top) = \sum_{i \in \mathcal{I}_k} \sum_{m=1}^M Q_{i,m}^{(k)} s_{i,m}^{(k)}, \\ \text{s.t.} \quad & \sum_{m=1}^M Q_{i,m}^{(k)} = 1, \quad \sum_{i \in \mathcal{I}_k} Q_{i,m}^{(k)} = \frac{B_k}{M}. \end{aligned} \quad (6)$$

These constraints enforce a balanced assignment of samples to prototypes. we apply the Sinkhorn–Knopp algorithm [Sinkhorn and Knopp, 1967] to solve this optimization problem [Cuturi, 2013]. We refine the prototype bank  $\mathcal{P}$  using a cross-entropy loss on labeled samples:

$$\mathcal{L}_{\text{P}} = \mathbb{E}_{k \in \mathcal{K}_v} \mathbb{E}_{i \in \mathcal{I}_k} \text{CE}(\mathbf{q}_i^{(k)}, \sigma(\frac{\mathbf{s}_i^{(k)}}{\epsilon})), \quad (7)$$

where  $\mathbb{E}$  denotes empirical averaging,  $\mathbf{s}_i^{(k)}, \mathbf{q}_i^{(k)} \in \mathbb{R}^M$  are the similarity vector to the class prototypes and the corresponding assignment, and  $\mathcal{K}_v = \{k \mid |\mathcal{I}_k^\ell| > 0\}$  denotes the set of classes that appear in the batch. The prototype label for each unlabeled sample is  $\hat{y}_j^{\text{proto}} = \arg \max_{k,m} s_{j,(k,m)}$ .

**Reliability Induction via Confidence-Aware Fusion.** Task priors emphasize inter-class separability, while prototype clustering captures intra-class variation. To leverage the complementary information and induce reliable pseudo-labels for EFM, we assign a pseudo-label  $\hat{y}_j$  only when the prior prediction  $\hat{y}_j^{\text{prior}}$  agrees with the prototype prediction  $\hat{y}_j^{\text{proto}}$ . We further quantify the reliability of agreed predictions using a confidence-aware fusion mechanism inspired by Dempster-Shafer theory [Deneœux, 2000].

**Lemma 3.2.** *In the singleton-only scenario and without ignorance mass, the Dempster-Shafer combination rule degenerates to  $m(\{\omega_c\}) = \frac{m_1(\{\omega_c\})m_2(\{\omega_c\})}{\sum_j m_1(\{\omega_j\})m_2(\{\omega_j\})}$ , where  $m_1(\cdot)$  and  $m_2(\cdot)$  denote the basic belief assignments (BBAs) provided by two evidence sources, and  $\omega_c \in \Omega$  represents the  $c$ -th singleton hypothesis in the frame of discernment  $\Omega$ .*

Under the setting of Lemma 3.2, we instantiate the two evidence sources as the task-prior prediction and the prototype-based prediction, respectively. Specifically, since both predictors output class-wise scores over singleton hypotheses and no explicit ignorance mass is modeled, their logits  $\mathbf{s}_j$  and  $\boldsymbol{\varpi}_j$  can be directly normalized to BBAs:

$$m_1^{(j)}(\cdot), m_2^{(j)}(\cdot) = \text{Softmax}(\mathbf{s}_j), \text{Softmax}(\boldsymbol{\varpi}_j), \quad (8)$$

The fused BBA  $m^{(j)}(\cdot)$  is obtained by combining  $m_1^{(j)}(\cdot)$  and  $m_2^{(j)}(\cdot)$  under the singleton-only assumption without ignorance mass. The confidence of the pseudo-label is then quantified using an entropy-based confidence score:

$$\gamma_j = 1 - \frac{-\sum_{c=1}^K m^{(j)}(\{\omega_k\}) \log m^{(j)}(\{\omega_k\})}{\log K}. \quad (9)$$

where  $K$  denotes the number of classes. An unlabeled sample  $\mathbf{X}_j$  is selected for adaptation only if its confidence score  $\gamma_j$  exceeds a predefined threshold  $\rho$ .

### 3.3 Prototype-Conditioned Adaptation

Building upon the constructed supervision, we propose a *Prototype-Conditioned Adapter (ProAdapter)* to utilize these signals for efficient adaptation. For each unlabeled sample  $\mathbf{X}_j \in \mathcal{D}_u$ , we use its prototype similarity vector  $\boldsymbol{\varpi}_j$  to condition lightweight adaptation modules inserted into a frozen EFM, enforcing a persistent structural constraint. The associated confidence score  $\gamma_j$  and pseudo-label  $\hat{y}_j$  are used to regulate the training objective for unlabeled data.

**Architecture.** *ProAdapter* adopts a feature-wise modulation design to adapt intermediate representations in a parameter-efficient manner, which is architecture-agnostic and operates on residual features when available and on layer outputs otherwise. In practice, *ProAdapter* is inserted into the last  $L$  layers of the backbone, as higher layers capture more abstract, task-relevant semantics, whereas lower layers mainly encode generic signal characteristics and are kept frozen.

**Prototype-Conditioned Modulation.** Given a prototype similarity  $\boldsymbol{\varpi}_j \in \mathbb{R}^K$  and an intermediate representation  $\mathbf{h}_l \in \mathbb{R}^{D \times T}$ , *ProAdapter* uses feature-wise modulation:

$$\text{ProAdapter}(\mathbf{h}_l; \boldsymbol{\varpi}_j) = \boldsymbol{\alpha}_j \odot \mathbf{h}_l + \boldsymbol{\beta}_j, \quad (10)$$

where  $\boldsymbol{\alpha}_j, \boldsymbol{\beta}_j \in \mathbb{R}^D$  are channel-wise scale and shift parameters, broadcast along the temporal dimension.

Modulation parameters are generated by a two-branch design. First, simple statistics from  $\mathbf{h}_l$  form a self-conditioning vector  $\mathbf{c}_j = [\boldsymbol{\mu}_l, \boldsymbol{\sigma}_l] = [\text{Mean}_t(\mathbf{h}_l), \text{Std}_t(\mathbf{h}_l)] \in \mathbb{R}^D$  to predict base modulation parameters:

$$[\Delta\boldsymbol{\alpha}_j^{(0)}; \boldsymbol{\beta}_j^{(0)}] = \text{Linear}(\mathbf{c}_j) \in \mathbb{R}^{2D}. \quad (11)$$

In parallel, the prototype similarity  $\boldsymbol{\varpi}_j$  produces an additional modulation term, whose magnitude is explicitly bounded and gated to ensure stable adaptation:

$$\begin{aligned} [\Delta\boldsymbol{\alpha}_j^{(\varpi)}; \boldsymbol{\beta}_j^{(\varpi)}] &= \lambda_\varpi \tanh(\text{Linear}(\boldsymbol{\varpi}_j)), \\ s_j &= \sigma(\text{Linear}(\boldsymbol{\varpi}_j)), \\ \Delta\boldsymbol{\alpha}_j &= \Delta\boldsymbol{\alpha}_j^{(0)} + s_j \Delta\boldsymbol{\alpha}_j^{(\varpi)}, \\ \boldsymbol{\beta}_j &= \boldsymbol{\beta}_j^{(0)} + s_j \boldsymbol{\beta}_j^{(\varpi)}, \\ \boldsymbol{\alpha}_j &= \mathbf{1} + \lambda \tanh(\Delta\boldsymbol{\alpha}_j), \end{aligned} \quad (12)$$

where  $\lambda_\varpi$  is a scaling factor. The modulated representation is then forwarded to the next layer of the frozen backbone.

### 3.4 Training Objective

We adopt a warm-up adaptation strategy that starts with supervised training on  $\mathcal{D}_l$ , and gradually incorporates unlabeled data for semi-supervised updates on  $\mathcal{D}_u$ . Each labeled mini-batch is paired with a fixed number of unlabeled samples to control the influence of pseudo-labels and prevent noisy supervision from dominating early training. Unlabeled data are sampled cyclically, so an epoch does not necessarily iterate over  $\mathcal{D}_u$ .

The semi-supervised loss is computed with sample-wise confidence weighting. For each unlabeled sample  $\mathbf{X}_j \in \mathcal{D}_u$ , a pseudo-label  $\hat{y}_j$  and a confidence score  $\gamma_j \in (0, 1)$  are obtained from the supervision construction, and a combined agreement-confidence mask  $m_j$  is applied. The resulting pseudo-supervised loss is defined as

$$\mathcal{L}_{\text{pseudo}} = \mathbb{E}_{\mathbf{X}_j \sim \mathcal{D}_u} m_j \gamma_j \text{CE}(\mathcal{F}_{\text{EFM}}(\mathbf{X}_j), \hat{y}_j). \quad (13)$$

The overall training objective is

$$\mathcal{L} = \mathcal{L}_{\text{sup}} + \mathcal{L}_{\text{pseudo}}, \quad (14)$$

where  $\text{CE}(\cdot, \cdot)$  denotes the standard cross-entropy loss, and  $\mathcal{L}_{\text{sup}}$  is computed on labeled samples in  $\mathcal{D}_l$ .

## 4 Experiments

### 4.1 Datasets

We evaluate our method on 3 public EEG datasets: **ISRU**C [Khalighi et al., 2016] for five-class sleep staging, **SEED** [Zheng and Lu, 2015] for binary emotion recognition, and **Mental Arithmetic** [Zyma et al., 2019] for binary mental workload assessment. For all datasets, we adopt a strict cross-subject setting, where 30% of training subjects are treated as labeled, with the remaining subjects used as unlabeled training data, while validation and test sets consist of held-out subjects unseen during training to mimic real-world label-limited data conditions. Specifically, for ISRUC dataset, subjects 1-24 are used for labeled training, 25-80 for unlabeled training, 81-90 for validation, and 91-100 for testing. For SEED dataset, subjects 1-3, 4-10, 11-12, and 13-15 are used for labeled training, unlabeled training, validation, and testing, respectively. For Mental Arithmetic dataset, subjects 1-7, 8-25, 26-30, and 31-35 are assigned to the same four splits. This subject-wise partitioning explicitly evaluates generalization under inter-subject distribution shifts. Additional dataset details are provided in Appendix C.3.

### 4.2 Experiment Settings

**Experiment Setup.** We evaluate our *SCOPE* framework as a plug-and-play adapter on multiple pretrained EFMs. Training is performed in two stages. In the first stage, we construct supervision using only the training data: labeled samples provide direct supervision, while unlabeled samples are used without labels to induce task priors, class prototypes, and confidence-aware pseudo-labels. In the second stage, all backbone parameters of pretrained EFMs are frozen, and only the proposed *ProAdapter* is optimized. Notably, the validation set is used only for model selection in the second stage and is not involved in any part of the first stage, while the test set is strictly held out throughout.

Across all backbone models, we adopt the same task-specific classifier head used in the original EFMs to ensure a fair comparison. Experiments are conducted on 40GB NVIDIA A100 GPUs. All models are trained using AdamW with a batch size of 64 and backbone-specific learning rates following its original setups. Results are reported as mean  $\pm$  standard deviation over 5 random seeds. For all backbone models, *ProAdapter* are inserted into the last three layers. We modulate transformer layer outputs and insert *ProAdapter* within residual layers for SSM-style backbones. Additional hyperparameter details are provided in Appendix J.

**Backbone and Baselines.** We evaluate the *SCOPE* framework on five publicly available EFMs, spanning different architectural designs. Specifically, we consider 3 transformer-based backbones (**LaBraM** [Jiang et al., 2024], **CBraMod** [Wang et al., 2025a], and **CSBrain** [Zhou et al., 2025c]) and 2 state-space-model (SSM)-style backbones (**EEGMamba** [Wang et al., 2025b] and **CodeBrain** [Ma et al., 2025c]).

As baselines, we include two representative task-specific EEG models, **EEGNet** [Lawhern et al., 2018] and **EEGConformer** [Song et al., 2022]. For foundation-model backbones, we report results under frozen and full fine-tuning settings as reference points, and further compare against parameter-efficient adaptation via **LoRA** [Hu et al., 2022] and two representative self-training semi-supervised frameworks, **FixMatch** [Sohn et al., 2020] and **FineSSL** [Gan and Wei, 2024]. Additional details are provided in Appendix E.

**Evaluation Metric.** Cohen’s Kappa and weighted F1 are reported for multiclass tasks, while AUROC and AUPRC are used for binary tasks. Model selection is based on Kappa or AUROC, and the best checkpoint is used for test evaluation. Additional metric definitions are provided in Appendix D.

Table 1: Baseline comparisons under the limited-label setting.

Backbone	Method	ISRUUC		SEED		Mental Arithmetic	
		Kappa	Weighted F1	AUPRC	AUROC	AUPRC	AUROC
<b>Non-Pretrained</b>	EEGNet	45.40±0.42	52.02±0.54	53.39±0.85	54.15±0.45	40.35±5.17	63.75±1.94
	EEGConformer	47.70±0.53	53.93±0.62	54.31±0.57	53.48±0.46	38.92±3.28	62.31±2.70
<i>Transformer-based backbones</i>							
<b>LaBraM</b>	Frozen	48.58±2.95	58.35±2.38	72.45±0.72	73.89±0.50	60.83±0.53	79.25±0.18
	+LoRA	<u>55.61</u> ±0.44	<u>65.05</u> ±0.36	67.51±3.34	57.28±8.43	<u>64.47</u> ±2.92	54.16±1.78
	+FixMatch <sup>†</sup>	33.14±1.29	43.83±2.49	<u>74.08</u> ±1.26	<b>77.32</b> ±1.48	53.92±12.48	74.41±7.56
	+FineSSL <sup>†</sup>	54.24±1.84	63.76±1.97	72.99±0.57	73.78±0.21	53.12±2.41	60.72±2.85
	+SCOPE (Ours) <sup>†</sup>	<b>56.19</b> ±0.67	<b>65.15</b> ±0.47	<b>74.25</b> ±0.44	<u>75.23</u> ±0.78	<b>64.64</b> ±2.49	<b>82.93</b> ±1.89
	Full finetuning	51.26±1.26	61.73±1.30	66.84±1.60	66.25±1.77	45.49±4.16	70.72±2.35
<b>CBraMod</b>	Frozen	60.34±0.93	67.91±0.78	57.83±2.60	58.74±2.10	47.19±0.86	63.53±1.32
	+LoRA	<u>63.16</u> ±1.17	<u>70.40</u> ±1.24	62.59±8.48	62.09±7.17	43.14±2.16	<u>70.45</u> ±0.91
	+FixMatch <sup>†</sup>	20.42±3.79	23.23±3.45	60.21±3.03	59.16±3.03	46.70±4.30	66.85±2.07
	+FineSSL <sup>†</sup>	53.46±1.97	61.21±2.27	57.84±1.31	58.42±3.31	41.51±7.61	64.43±2.41
	+SCOPE (Ours) <sup>†</sup>	<b>63.29</b> ±1.12	<b>70.74</b> ±0.64	<b>65.57</b> ±1.86	<u>63.71</u> ±1.82	<b>54.44</b> ±0.73	<b>74.39</b> ±0.98
	Full finetuning	61.95±1.02	69.78±0.95	<u>65.12</u> ±2.39	<b>64.43</b> ±2.73	<u>47.35</u> ±2.75	69.91±2.72
<b>CSBrain</b>	Frozen	56.27±1.49	64.98±1.16	56.27±0.43	56.57±0.62	38.30±1.76	66.68±0.87
	+LoRA	60.30±0.69	68.56±0.80	56.98±0.36	<u>57.45</u> ±0.49	33.78±0.38	63.24±0.38
	+FixMatch <sup>†</sup>	44.53±1.59	53.48±2.27	59.71±0.76	57.34±0.95	<u>43.24</u> ±1.89	69.13±0.60
	+FineSSL <sup>†</sup>	47.65±0.62	54.61±0.44	53.46±1.05	53.86±1.27	36.41±1.05	66.35±1.86
	+SCOPE (Ours) <sup>†</sup>	<b>61.51</b> ±0.55	<b>69.86</b> ±0.69	<b>63.05</b> ±0.59	<b>62.09</b> ±0.66	<b>47.60</b> ±0.83	<b>71.09</b> ±1.04
	Full finetuning	60.97±1.04	69.19±1.09	57.54±3.08	57.40±2.22	40.08±5.68	67.39±2.74
<i>SSM-style backbones</i>							
<b>EEGMamba</b>	Frozen	60.73±0.67	67.94±1.11	58.27±0.75	57.30±0.67	37.19±1.01	64.98±1.30
	+LoRA	<u>62.78</u> ±1.02	<u>69.79</u> ±0.48	58.64±1.38	57.35±1.32	38.12±0.93	65.45±0.81
	+FixMatch <sup>†</sup>	32.00±1.93	44.07±1.25	58.86±0.82	57.67±1.07	42.61±1.47	<u>67.61</u> ±1.06
	+FineSSL <sup>†</sup>	54.02±7.36	65.92±1.90	48.98±0.80	47.64±1.37	39.11±1.73	66.86±0.72
	+SCOPE (Ours) <sup>†</sup>	<b>63.07</b> ±0.89	<b>71.41</b> ±0.79	<b>60.65</b> ±0.50	<b>59.02</b> ±0.52	<b>49.46</b> ±0.18	<b>68.48</b> ±0.34
	Full finetuning	62.02±0.87	68.71±0.91	<u>59.84</u> ±1.03	<u>57.98</u> ±0.93	<u>42.89</u> ±2.73	65.36±1.15
<b>CodeBrain</b>	Frozen	52.54±1.40	61.75±1.25	63.44±1.54	<u>63.93</u> ±2.06	46.70±2.09	71.25±2.72
	+LoRA	44.08±6.73	53.37±6.49	63.83±2.67	58.61±3.38	44.05±0.84	68.49±1.32
	+FixMatch <sup>†</sup>	57.23±0.64	66.74±0.51	61.58±1.19	60.58±0.82	44.53±2.07	69.30±1.31
	+FineSSL <sup>†</sup>	48.94±0.83	57.50±0.96	63.72±0.93	62.85±0.59	<u>47.14</u> ±4.08	71.25±2.83
	+SCOPE (Ours) <sup>†</sup>	<b>63.46</b> ±0.98	<b>71.11</b> ±0.74	<b>65.88</b> ±0.51	<b>65.30</b> ±0.45	<b>49.30</b> ±1.02	<b>72.40</b> ±0.70
	Full finetuning	58.46±1.42	67.05±1.57	64.30±3.83	63.27±4.75	47.10±2.09	72.13±2.72

\* LaBraM is pretrained on cohorts including the SEED dataset. <sup>†</sup> Methods also use unlabeled data for semi-supervised training.

### 4.3 Performance Comparison.

Table 1 summarizes results under the limited-label setting, where the best results are highlighted in **bold**, the second-best results are underlined, and our method is color-coded. Across all five backbones and three datasets, our method consistently achieves strong performance, outperforming the frozen backbone and generally surpassing full fine-tuning. For example, compared with frozen backbones, on ISRUUC we improve Kappa by +7.61 with LaBraM and +10.92 with CodeBrain; on SEED, we improve AUPRC by +6.78 with CSBrain; and on Mental Arithmetic, we improve AUPRC by +12.27 with EEGMamba. These gains are consistently observed across Transformer-based and SSM-style backbones, indicating that *SCOPE* generalizes well across different architectural families under cross-subject distribution shifts.

Notably, these gains are obtained with only 2-5% trainable parameters, substantially fewer than full fine-tuning, and with significantly reduced training time and GPU memory usage. While operating in a parameter-efficient regime comparable to LoRA, *SCOPE* consistently yields stronger performance. Detailed statistics are reported in Appendix G.

Table 2: Ablation on ISRUC with partial labels. Methods marked with  $\dagger$  additionally use pseudo-labeled data for semi-supervised training.

Method	CSBrain (Transformer-based Backbone)				CodeBrain (SSM-Style Backbone)			
	Kappa	$\Delta\%$	Weighted-F1	$\Delta\%$	Kappa	$\Delta\%$	Weighted-F1	$\Delta\%$
Frozen	56.27 $\pm$ 1.49	–	64.98 $\pm$ 1.16	–	52.54 $\pm$ 1.40	–	61.75 $\pm$ 1.25	–
<i>Ablation on Supervision Construction</i>								
w/o ETF-guide $\dagger$	60.04 $\pm$ 2.39	$\downarrow$ 2.38%	68.15 $\pm$ 2.07	$\downarrow$ 2.45%	61.48 $\pm$ 1.72	$\downarrow$ 3.12%	68.87 $\pm$ 1.35	$\downarrow$ 3.15%
w/o Prototype Clustering $\dagger$	59.16 $\pm$ 1.24	$\downarrow$ 3.82%	67.53 $\pm$ 1.32	$\downarrow$ 3.33%	60.76 $\pm$ 0.94	$\downarrow$ 4.25%	67.91 $\pm$ 0.86	$\downarrow$ 4.50%
w/o Supervision construction	58.30 $\pm$ 1.63	$\downarrow$ 5.22%	66.74 $\pm$ 1.51	$\downarrow$ 4.47%	59.01 $\pm$ 1.45	$\downarrow$ 7.01%	66.78 $\pm$ 1.03	$\downarrow$ 6.09%
<i>Ablation on ProAdapter Design</i>								
w/o <i>ProAdapter</i> $\dagger$	58.49 $\pm$ 0.76	$\downarrow$ 4.91%	66.52 $\pm$ 0.78	$\downarrow$ 4.78%	56.96 $\pm$ 0.52	$\downarrow$ 10.25%	64.46 $\pm$ 0.77	$\downarrow$ 9.35%
w/o Confidence Weights $\dagger$	60.35 $\pm$ 0.93	$\downarrow$ 1.89%	67.85 $\pm$ 1.04	$\downarrow$ 2.88%	61.75 $\pm$ 1.18	$\downarrow$ 2.69%	69.22 $\pm$ 1.34	$\downarrow$ 2.66%
w/o Prototype Conditioning $\dagger$	58.66 $\pm$ 1.35	$\downarrow$ 4.63%	66.59 $\pm$ 1.10	$\downarrow$ 4.68%	59.60 $\pm$ 1.33	$\downarrow$ 6.08%	66.97 $\pm$ 1.46	$\downarrow$ 5.82%
<i>Ablation on Training Strategy</i>								
w/o Warm-up $\dagger$	59.29 $\pm$ 0.62	$\downarrow$ 3.61%	67.46 $\pm$ 0.77	$\downarrow$ 3.44%	61.84 $\pm$ 1.05	$\downarrow$ 2.55%	69.12 $\pm$ 1.26	$\downarrow$ 2.80%
sequential $\dagger$	59.20 $\pm$ 1.16	$\downarrow$ 3.76%	67.67 $\pm$ 1.21	$\downarrow$ 3.14%	58.28 $\pm$ 1.08	$\downarrow$ 8.16%	66.53 $\pm$ 1.35	$\downarrow$ 6.44%
Two-Stage $\dagger$	58.31 $\pm$ 0.45	$\downarrow$ 5.20%	66.42 $\pm$ 0.69	$\downarrow$ 4.93%	57.10 $\pm$ 1.29	$\downarrow$ 10.02%	64.60 $\pm$ 1.10	$\downarrow$ 9.16%
<b>SCOPE (Our full model) <math>\dagger</math></b>	<b>61.51<math>\pm</math>0.55</b>	–	<b>69.86<math>\pm</math>0.69</b>	–	<b>63.46<math>\pm</math>1.98</b>	–	<b>71.11<math>\pm</math>0.74</b>	–

#### 4.4 Ablation Study

We conduct ablation studies on ISRUC dataset using *CSBrain* and *CodeBrain* as representative backbones of different architectures. Table 2 summarizes the results grouped by core components and training strategy.

**1) Ablation on Supervision Construction.** We progressively remove components from the supervision construction module. Removing ETF guidance (**w/o ETF-guide**) causes consistent 2-3% drops, while discarding prototype clustering (**w/o Prototype Clustering**) leads to larger degradations of 3-5%. Disabling supervision construction entirely (**w/o Supervision construction**) results in the largest performance loss (5-7%), indicating that adapting the backbone with the adapter alone, without any constructed supervision, provides insufficient structure guidance.

**2) Ablation on ProAdapter Design.** Removing *ProAdapter* (**w/o ProAdapter**) reduces the method to self-training on a frozen backbone and causes the largest performance drops across both backbones, particularly on CodeBrain (up to 9-10%). This indicates that *ProAdapter* enables adaptation, with stronger effects on SSM-style backbones, possibly due to effective residual-layer modulation by the adapter. Removing prototype conditioning (**w/o Prototype Conditioning**) leads to 4-6% degradations, indicating the necessity of structured, persistent supervision to continuously guide the adaptation. Discarding confidence weighting (**w/o Confidence Weights**) results in smaller but consistent drops (2-3%), demonstrating that suppressing unreliable samples during optimization is important for stabilizing adaptation.

**3) Ablation on Training Strategy.** Removing the supervised warm-up (**w/o Warm-up**) degrades performance, showing that an initial ground-truth-only phase is necessary. The **Sequential** strategy processes labeled samples before unlabeled ones within each epoch and further reduces performance, indicating that pseudo-labeled updates require tight anchoring by labeled supervision. The **Two-Stage** strategy, which trains on labeled data followed by unlabeled data only, causes the largest drop; performance often peaks during the supervised phase, suggesting limited benefit from pseudo-labeled data when supervision is fully decoupled.

#### 4.5 Sensitivity Analysis

We analyze the sensitivity of *ProAdapter* to the adapter depth and the confidence threshold  $\rho$  for selecting pseudo-labeled samples on ISRUC, using *CSBrain* and *CodeBrain* as representative backbones of different architectures.

**1) Sensitivity to ProAdapter Depth.** Figure 4 analyzes the sensitivity of *ProAdapter* to the adapter depth  $L$ , where adapters are inserted into the last  $L$  layers of the backbone. Performance exhibits a non-monotonic trend as  $L$  increases, first improving, then saturating, and potentially degrading as adaptation becomes deeper. The deeper Transformer-based *CSBrain* (12 layers) exhibits sharper degradation under excessive adaptation, whereas the shallower SSM-based *CodeBrain* (8 layers) remains more robust. To balance performance and efficiency, we adopt a unified adapter depth of three layers across all backbones and tasks.

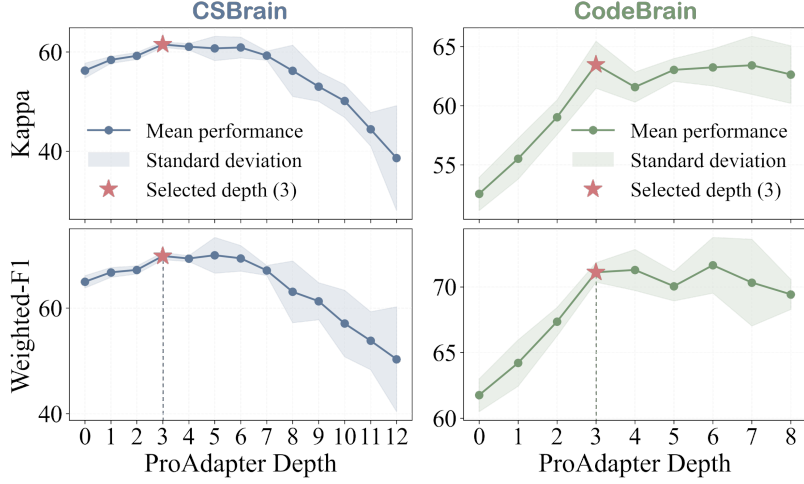


Figure 4: Sensitivity analysis of *ProAdapter* depth on ISRUC.

**2) Sensitivity to Confidence Threshold.** We analyze the sensitivity to the confidence threshold  $\rho$ , where only unlabeled samples with confidence greater than  $\rho$  are included for adaptation. Figure 5 shows that both models exhibit a clear trade-off: low thresholds admit noise and degrade performance, whereas overly high thresholds restrict supervision to only easy samples and reduce data coverage. Based on this, we set  $\rho = 0.5$  for all backbones and tasks.

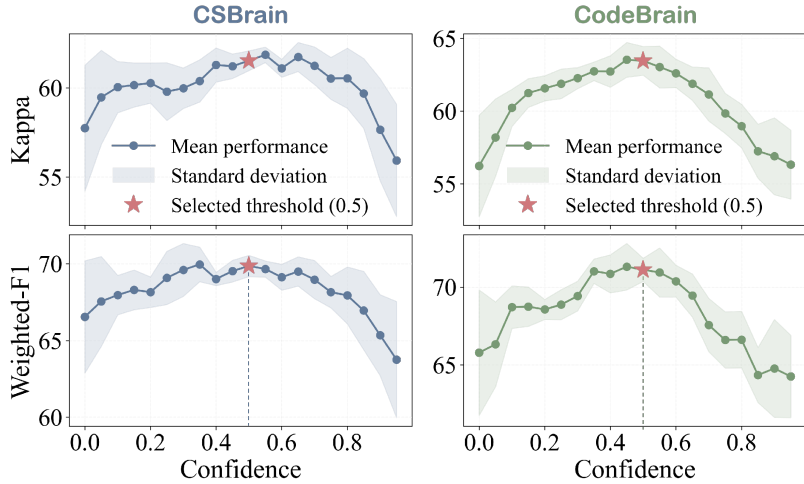


Figure 5: Sensitivity analysis of confidence threshold on ISRUC.

The results and additional analyzes on the *number of prototypes per class*, *ETF loss weight*, *pseudo-labeled data ratio*, and *pseudo-label quality* in Appendix F and H.

## 5 Conclusion

We propose *SCOPE*, a prototype-guided adaptation framework for EEG foundation models that constructs external supervision and modulates the last layers via structured prototypes, achieving consistent gains across 3 tasks and 5 backbones. We hope this work advances practical deployment of EEG foundation models in real-world settings.

## References

Ahmed Waleed Al-Asadi, Pedram Salehpour, and Hadi S Aghdasi. A robust semi-supervised deep learning approach for emotion recognition using eeg signals. *International Journal of Machine Learning and Cybernetics*, 15(10):4445–4458, 2024.

Irfan Al-Hussaini, Cao Xiao, M Brandon Westover, and Jimeng Sun. Sleeper: interpretable sleep staging via prototypes from expert rules. In *Machine Learning for Healthcare Conference*, pages 721–739. PMLR, 2019.

Richard B Berry, Rita Brooks, Charlene Gamaldo, Susan M Harding, Robin M Lloyd, Stuart F Quan, Matthew T Troester, and Bradley V Vaughn. Aasm scoring manual updates for 2017 (version 2.4), 2017.

David Berthelot, Nicholas Carlini, Ian Goodfellow, Nicolas Papernot, Avital Oliver, and Colin A Raffel. Mixmatch: A holistic approach to semi-supervised learning. *Advances in neural information processing systems*, 32, 2019.

David Berthelot, Nicholas Carlini, Ekin D Cubuk, Alex Kurakin, Kihyuk Sohn, Han Zhang, and Colin Raffel. Remixmatch: Semi-supervised learning with distribution matching and augmentation anchoring. In *International Conference on Learning Representations*, 2020.

Donghong Cai, Junru Chen, Yang Yang, Teng Liu, and Yafeng Li. Mbrain: A multi-channel self-supervised learning framework for brain signals. In *Proceedings of the 29th ACM SIGKDD Conference on Knowledge Discovery and Data Mining*, pages 130–141, 2023.

Mathilde Caron, Ishan Misra, Julien Mairal, Priya Goyal, Piotr Bojanowski, and Armand Joulin. Unsupervised learning of visual features by contrasting cluster assignments. *Advances in neural information processing systems*, 33:9912–9924, 2020.

Junru Chen, Yang Yang, Tao Yu, Yingying Fan, Xiaolong Mo, and Carl Yang. Brainnet: Epileptic wave detection from seeg with hierarchical graph diffusion learning. In *Proceedings of the 28th ACM SIGKDD conference on knowledge discovery and data mining*, pages 2741–2751, 2022.

Zhisheng Chen, Yingwei Zhang, Qizhen Lan, Tianyu Liu, Huacan Wang, Yi Ding, Ziyu Jia, Ronghao Chen, Kun Wang, and Xinliang Zhou. Uni-ntfm: A unified foundation model for eeg signal representation learning. *arXiv preprint arXiv:2509.24222*, 2025.

Hsiang-Yun Sherry Chien, Hanlin Goh, Christopher Michael Sandino, and Joseph Yitan Cheng. Maeeg: Masked auto-encoder for eeg representation learning. In *NeurIPS 2022 Workshop on Learning from Time Series for Health*, 2022.

Wenhui Cui, Woojae Jeong, Philipp Thölke, Takfarinas Medani, Karim Jerbi, Anand A Joshi, and Richard M Leahy. Neuro-gpt: Towards a foundation model for eeg. In *2024 IEEE International Symposium on Biomedical Imaging (ISBI)*, pages 1–5. IEEE, 2024.

Marco Cuturi. Sinkhorn distances: Lightspeed computation of optimal transport. *Advances in neural information processing systems*, 26, 2013.

Chenglong Dai, Jia Wu, Jessica JM Monaghan, Guanghui Li, Hao Peng, Stefanie I Becker, and David McAlpine. Semi-supervised eeg clustering with multiple constraints. *IEEE Transactions on Knowledge and Data Engineering*, 35(8):8529–8544, 2022.

Thierry Denœux. A neural network classifier based on Dempster–Shafer theory. *IEEE Transactions on Systems, Man, and Cybernetics-Part A: Systems and Humans*, 30(2):131–150, 2000.

Thierry Denœux. Quantifying prediction uncertainty in regression using random fuzzy sets: the ennreg model. *IEEE Transactions on Fuzzy Systems*, 31(10):3690–3699, 2023a.

Thierry Denœux. Reasoning with fuzzy and uncertain evidence using epistemic random fuzzy sets: General framework and practical models. *Fuzzy Sets and Systems*, 453:1–36, 2023b.

Ning Ding, Yujia Qin, Guang Yang, Fuchao Wei, Zonghan Yang, Yusheng Su, Shengding Hu, Yulin Chen, Chi-Min Chan, Weize Chen, et al. Parameter-efficient fine-tuning of large-scale pre-trained language models. *Nature machine intelligence*, 5(3):220–235, 2023.

Yidan Ding, Chalisa Udompanyawit, Yisha Zhang, and Bin He. Eeg-based brain-computer interface enables real-time robotic hand control at individual finger level. *Nature Communications*, 16(1):1–20, 2025.

Zitao Fang, CHENXUAN LI, Zhou Hongting, Shuyang Yu, Guodong DU, Ashwaq Qasem, Yang Lu, Jing Li, Junsong Zhang, and Sim Kuan Goh. Neuript: Foundation model for neural interfaces. In *The Thirty-ninth Annual Conference on Neural Information Processing Systems*, 2025.

Kai Gan and Tong Wei. Erasing the bias: fine-tuning foundation models for semi-supervised learning. In *Proceedings of the 41st International Conference on Machine Learning*, pages 14453–14470, 2024.

Robert Geirhos, Jörn-Henrik Jacobsen, Claudio Michaelis, Richard Zemel, Wieland Brendel, Matthias Bethge, and Felix A Wichmann. Shortcut learning in deep neural networks. *Nature Machine Intelligence*, 2(11):665–673, 2020.

Lan-Zhe Guo and Yu-Feng Li. Class-imbalanced semi-supervised learning with adaptive thresholding. In *International conference on machine learning*, pages 8082–8094. PMLR, 2022.

Bo Han, Quanming Yao, Xingrui Yu, Gang Niu, Miao Xu, Weihua Hu, Ivor Tsang, and Masashi Sugiyama. Co-teaching: Robust training of deep neural networks with extremely noisy labels. *Advances in neural information processing systems*, 31, 2018.

Neil Houlsby, Andrei Giurgiu, Stanislaw Jastrzebski, Bruna Morrone, Quentin De Laroussilhe, Andrea Gesmundo, Mona Attariyan, and Sylvain Gelly. Parameter-efficient transfer learning for nlp. In *International conference on machine learning*, pages 2790–2799. PMLR, 2019.

Edward J Hu, Yelong Shen, Phillip Wallis, Zeyuan Allen-Zhu, Yuanzhi Li, Shean Wang, Lu Wang, Weizhu Chen, et al. Lora: Low-rank adaptation of large language models. *ICLR*, 1(2):3, 2022.

Ling Huang, Su Ruan, Pierre Decazes, and Thierry Denceux. Lymphoma segmentation from 3d pet-ct images using a deep evidential network. *International Journal of Approximate Reasoning*, 149:39–60, 2022.

Ling Huang, Su Ruan, Yucheng Xing, and Mengling Feng. A review of uncertainty quantification in medical image analysis: Probabilistic and non-probabilistic methods. *Medical Image Analysis*, 97:103223, 2024a.

Ling Huang, Yucheng Xing, Thierry Denoeux, and Mengling Feng. An evidential time-to-event prediction model based on gaussian random fuzzy numbers. In *International Conference on Belief Functions*, pages 49–57. Springer, 2024b.

Ling Huang, Su Ruan, Pierre Decazes, and Thierry Denceux. Deep evidential fusion with uncertainty quantification and reliability learning for multimodal medical image segmentation. *Information Fusion*, 113:102648, 2025a.

Ling Huang, Yucheng Xing, Qika Lin, Jinming Duan, Su Ruan, and Mengling Feng. Esurvfusion: An evidential multimodal survival fusion model based on epistemic random fuzzy sets. *IEEE Transactions on Fuzzy Systems*, 2025b.

Ling Huang, Yucheng Xing, Swapnil Mishra, Thierry Denoeux, and Mengling Feng. Evidential time-to-event prediction with calibrated uncertainty quantification. *International Journal of Approximate Reasoning*, 181:109403, 2025c.

Weixuan Huang, Yan Wang, Hanrong Cheng, Wei Xu, Tingyue Li, Xiuwen Wu, Hui Xu, Pan Liao, Zaixu Cui, Qihong Zou, et al. A unified time-frequency foundation model for sleep decoding. *Nature Communications*, 2026.

Neel Jain, Ping-yeh Chiang, Yuxin Wen, John Kirchenbauer, Hong-Min Chu, Gowthami Somepalli, Brian R Bartoldson, Bhavya Kailkhura, Avi Schwarzschild, Aniruddha Saha, et al. Neptune: Noisy embeddings improve instruction finetuning. In *The Twelfth International Conference on Learning Representations*, 2024.

Jaehyun Jeon, Seungwoo Jeong, Yeajin Shon, and Heung-II Suk. Parameter-efficient transfer learning for eeg foundation models via task-relevant feature focusing. In *Proceedings of the 34th ACM International Conference on Information and Knowledge Management*, pages 1068–1077, 2025.

Weibang Jiang, Liming Zhao, and Bao-liang Lu. Large brain model for learning generic representations with tremendous eeg data in bci. In *The Twelfth International Conference on Learning Representations*, 2024.

Weibang Jiang, Yansen Wang, Bao-liang Lu, and Dongsheng Li. Neurolm: A universal multi-task foundation model for bridging the gap between language and eeg signals. In *The Thirteenth International Conference on Learning Representations*, 2025.

Xue Jiang, Lubin Meng, Ziwei Wang, and Dongrui Wu. Deep source semi-supervised transfer learning (ds3tl) for cross-subject eeg classification. *IEEE Transactions on Biomedical Engineering*, 71(4):1308–1318, 2023.

Jin Jing, Aline Herlopian, Ioannis Karakis, Marcus Ng, Jonathan J Halford, Alice Lam, Douglas Maus, Fonda Chan, Marjan Dolatshahi, Carlos F Muniz, et al. Interrater reliability of experts in identifying interictal epileptiform discharges in electroencephalograms. *JAMA neurology*, 77(1):49–57, 2020.

Antonis Karantonis, Konstantinos Barmpas, Dimitrios Adamos, Nikolaos Laskaris, Stefanos Zafeiriou, and Yannis Panagakis. Subject-aware contrastive learning for eeg foundation models. In *NeurIPS 2025 Workshop on Learning from Time Series for Health*, 2025.

Rabeeh Karimi Mahabadi, James Henderson, and Sebastian Ruder. Compacter: Efficient low-rank hypercomplex adapter layers. *Advances in neural information processing systems*, 34:1022–1035, 2021.

Sirvan Khalighi, Teresa Sousa, José Moutinho Santos, and Urbano Nunes. Isruc-sleep: A comprehensive public dataset for sleep researchers. *Computer methods and programs in biomedicine*, 124:180–192, 2016.

Demetres Kostas, Stephane Aroca-Ouellette, and Frank Rudzicz. Bendlr: Using transformers and a contrastive self-supervised learning task to learn from massive amounts of eeg data. *Frontiers in Human Neuroscience*, 15:653659, 2021.

Ananya Kumar, Aditi Raghunathan, Robbie Matthew Jones, Tengyu Ma, and Percy Liang. Fine-tuning can distort pretrained features and underperform out-of-distribution. In *International Conference on Learning Representations*, 2022.

Vernon J Lawhern, Amelia J Solon, Nicholas R Waytowich, Stephen M Gordon, Chou P Hung, and Brent J Lance. Eegnet: a compact convolutional neural network for eeg-based brain–computer interfaces. *Journal of neural engineering*, 15(5):056013, 2018.

Andrew S Lea and David S Jones. Mind the gap—machine learning, dataset shift, and history in the age of clinical algorithms. *New England Journal of Medicine*, 390(4):293–295, 2024.

Na Lee, Konstantinos Barmpas, Yannis Panagakis, Dimitrios Adamos, Nikolaos Laskaris, and Stefanos Zafeiriou. Are large brainwave foundation models capable yet? insights from fine-tuning. *arXiv preprint arXiv:2507.01196*, 2025.

Chenyu Liu, Xinliang Zhou, Zhengri Zhu, Liming Zhai, Ziyu Jia, and Yang Liu. Vbh-gnn: Variational bayesian heterogeneous graph neural networks for cross-subject emotion recognition. In *The Twelfth International Conference on Learning Representations*, 2024.

Chenyu Liu, Yuqiu Deng, Tianyu Liu, Jinan Zhou, Xinliang Zhou, Ziyu Jia, and Yi Ding. Echo: Toward contextual seq2seq paradigms in large eeg models. *arXiv preprint arXiv:2509.22556*, 2025.

Haokun Liu, Derek Tam, Mohammed Muqeeth, Jay Mohta, Tenghao Huang, Mohit Bansal, and Colin A Raffel. Few-shot parameter-efficient fine-tuning is better and cheaper than in-context learning. *Advances in Neural Information Processing Systems*, 35:1950–1965, 2022.

Stuart Lloyd. Least squares quantization in pcm. *IEEE transactions on information theory*, 28(2):129–137, 1982.

Weiheng Lu, Chunfeng Song, Jiamin Wu, Pengyu Zhu, Yuchen Zhou, Weijian Mai, Qihao Zheng, and Wanli Ouyang. Unimind: Unleashing the power of llms for unified multi-task brain decoding. *arXiv preprint arXiv:2506.18962*, 2025.

Jingying Ma, Qika Lin, Ziyu Jia, and Mengling Feng. St-usleepnet: A spatial-temporal coupling prominence network for multi-channel sleep staging. In *Proceedings of the Thirty-Fourth International Joint Conference on Artificial Intelligence*, pages 4182–4190, 2025a.

Jingying Ma, Jinwei Wang, Lanlan Lu, Yexiang Sun, Mengling Feng, Feifei Zhang, Peng Shen, Zhiqin Jiang, Shenda Hong, and Luxia Zhang. Development and validation of a dynamic kidney failure prediction model based on deep learning: A real-world study with external validation. *arXiv preprint arXiv:2501.16388*, 2025b.

Jingying Ma, Feng Wu, Qika Lin, Yucheng Xing, Chenyu Liu, Ziyu Jia, and Mengling Feng. Codebrain: Towards decoupled interpretability and multi-scale architecture for eeg foundation model. *arXiv preprint arXiv:2506.09110*, 2025c.

Rabeeh Karimi Mahabadi, Sebastian Ruder, Mostafa Dehghani, and James Henderson. Parameter-efficient multi-task fine-tuning for transformers via shared hypernetworks. In Chengqing Zong, Fei Xia, Wenjie Li, and Roberto Navigli, editors, *Proceedings of the 59th Annual Meeting of the Association for Computational Linguistics and the 11th International Joint Conference on Natural Language Processing, ACL/IJCNLP 2021, (Volume 1: Long Papers), Virtual Event, August 1-6, 2021*, pages 565–576. Association for Computational Linguistics, 2021. doi: 10.18653/V1/2021.ACL-LONG.47. URL <https://doi.org/10.18653/v1/2021.acl-long.47>.

Navid Mohammadi Foumani, Geoffrey Mackellar, Soheila Ghane, Saad Irtza, Nam Nguyen, and Mahsa Salehi. Eeg2rep: enhancing self-supervised eeg representation through informative masked inputs. In *Proceedings of the 30th ACM SIGKDD Conference on Knowledge Discovery and Data Mining*, pages 5544–5555, 2024.

Faisal Mushtaq, Dominik Welke, Anne Gallagher, Yuri G Pavlov, Layla Kouara, Jorge Bosch-Bayard, Jasper JF van den Bosch, Mahnaz Arvaneh, Amy R Bland, Maximilien Chaumon, et al. One hundred years of eeg for brain and behaviour research. *Nature human behaviour*, 8(8):1437–1443, 2024.

Hamid Niknazar and Sara C Mednick. A multi-level interpretable sleep stage scoring system by infusing experts' knowledge into a deep network architecture. *IEEE transactions on pattern analysis and machine intelligence*, 46(7):5044–5061, 2024.

Iyad Obeid and Joseph Picone. The temple university hospital eeg data corpus. *Frontiers in neuroscience*, 10:196, 2016.

Vardan Papyan, XY Han, and David L Donoho. Prevalence of neural collapse during the terminal phase of deep learning training. *Proceedings of the National Academy of Sciences*, 117(40):24652–24663, 2020.

Jacob Pellinen, Emma C Foster, Jo M Wilmshurst, Sameer M Zuberi, and Jacqueline French. Improving epilepsy diagnosis across the lifespan: approaches and innovations. *The Lancet Neurology*, 23(5):511–521, 2024.

Ethan Perez, Florian Strub, Harm De Vries, Vincent Dumoulin, and Aaron Courville. Film: Visual reasoning with a general conditioning layer. In *Proceedings of the AAAI conference on artificial intelligence*, volume 32, 2018.

Sen Qiu, Yongtao Chen, Yulin Yang, Pengfei Wang, Zhelong Wang, Hongyu Zhao, Yuntong Kang, and Ruicheng Nie. A review on semi-supervised learning for eeg-based emotion recognition. *Information Fusion*, 104:102190, 2024.

Mamshad Nayeem Rizve, Kevin Duarte, Yogesh S Rawat, and Mubarak Shah. In defense of pseudo-labeling: An uncertainty-aware pseudo-label selection framework for semi-supervised learning. In *International Conference on Learning Representations*, 2021.

Sunny Sanyal, Hayden Prairie, Rudrajit Das, Ali Kavis, and Sujay Sanghavi. Upweighting easy samples in fine-tuning mitigates forgetting. In *Forty-second International Conference on Machine Learning*, 2025.

Glenn Shafer. Dempster-shafer theory. *Encyclopedia of artificial intelligence*, 1:330–331, 1992.

Afshin Shoeibi, Marjane Khodatars, Navid Ghassemi, Mahboobeh Jafari, Parisa Moridian, Roohallah Alizadehsani, Maryam Panahiazar, Fahime Khozeimeh, Assef Zare, Hossein Hosseini-Nejad, et al. Epileptic seizures detection using deep learning techniques: a review. *International journal of environmental research and public health*, 18(11):5780, 2021.

Richard Sinkhorn and Paul Knopp. Concerning nonnegative matrices and doubly stochastic matrices. *Pacific Journal of Mathematics*, 21(2):343–348, 1967.

Jake Snell, Kevin Swersky, and Richard Zemel. Prototypical networks for few-shot learning. *Advances in neural information processing systems*, 30, 2017.

Kihyuk Sohn, David Berthelot, Nicholas Carlini, Zizhao Zhang, Han Zhang, Colin A Raffel, Ekin Dogus Cubuk, Alexey Kurakin, and Chun-Liang Li. Fixmatch: Simplifying semi-supervised learning with consistency and confidence. *Advances in neural information processing systems*, 33:596–608, 2020.

Yonghao Song, Qingqing Zheng, Bingchuan Liu, and Xiaorong Gao. Eeg conformer: Convolutional transformer for eeg decoding and visualization. *IEEE Transactions on Neural Systems and Rehabilitation Engineering*, 31: 710–719, 2022.

Jingnan Sun, Anruo Shen, Yike Sun, Xiaogang Chen, Yunxia Li, Xiaorong Gao, and Bai Lu. Adaptive spatiotemporal encoding network for cognitive assessment using resting state eeg. *npj Digital Medicine*, 7(1):375, 2024.

Dennis Tang, Jon Donnelly, Alina Jade Barnett, Lesia Semenova, Jin Jing, Peter Hadar, Ioannis Karakis, Olga Selioutski, Kehan Zhao, M Brandon Westover, et al. This eeg looks like these eegs: Interpretable interictal epileptiform discharge detection with protoeeg-knn. In *International Conference on Medical Image Computing and Computer-Assisted Intervention*, pages 615–625. Springer, 2025.

Zheng Tong, Philippe Xu, and Thierry Denoeux. An evidential classifier based on dempster-shafer theory and deep learning. *Neurocomputing*, 450:275–293, 2021.

Shihao Tu, Linfeng Cao, Daoze Zhang, Junru Chen, Lvbin Ma, Yin Zhang, and Yang Yang. Dmnet: Self-comparison driven model for subject-independent seizure detection. *Advances in Neural Information Processing Systems*, 37: 28254–28280, 2024.

Jesper E Van Engelen and Holger H Hoos. A survey on semi-supervised learning. *Machine learning*, 109(2):373–440, 2020.

Guangyu Wang, Wenchao Liu, Yuhong He, Cong Xu, Lin Ma, and Haifeng Li. Eegpt: Pretrained transformer for universal and reliable representation of eeg signals. *Advances in Neural Information Processing Systems*, 37: 39249–39280, 2024.

Jiquan Wang, Sha Zhao, Zhiling Luo, Yangxuan Zhou, Haiteng Jiang, Shijian Li, Tao Li, and Gang Pan. Cbramod: A criss-cross brain foundation model for eeg decoding. In *The Thirteenth International Conference on Learning Representations*, 2025a.

Jiquan Wang, Sha Zhao, Zhiling Luo, Yangxuan Zhou, Shijian Li, and Gang Pan. Eegmamba: An eeg foundation model with mamba. *Neural Networks*, page 107816, 2025b.

Jiquan Wang, Sha Zhao, Yangxuan Zhou, Yiming Kang, Shijian Li, and Gang Pan. Deeperbrain: A neuro-grounded eeg foundation model towards universal bci. *arXiv preprint arXiv:2601.06134*, 2026a.

Yidong Wang, Hao Chen, Qiang Heng, Wenxin Hou, Yue Fan, Zhen Wu, Jindong Wang, Marios Savvides, Takahiro Shinozaki, Bhiksha Raj, et al. Freematch: Self-adaptive thresholding for semi-supervised learning. In *The Eleventh International Conference on Learning Representations*, 2022.

Yihe Wang, Zhiqiao Kang, Bohan Chen, Yu Zhang, and Xiang Zhang. Benchmarking erp analysis: Manual features, deep learning, and foundation models. *arXiv preprint arXiv:2601.00573*, 2026b.

Weining Weng, Yang Gu, Shuai Guo, Yuan Ma, Zhaohua Yang, Yuchen Liu, and Yiqiang Chen. Self-supervised learning for electroencephalogram: A systematic survey. *ACM Computing Surveys*, 57(12):1–38, 2025.

Chuhan Wu, Fangzhao Wu, Tao Qi, and Yongfeng Huang. Noisytune: A little noise can help you finetune pretrained language models better. In *Proceedings of the 60th Annual Meeting of the Association for Computational Linguistics (Volume 2: Short Papers)*, pages 680–685, 2022.

Qinfan Xiao, Ziyun Cui, Chi Zhang, Siqi Chen, Wen Wu, Andrew Thwaites, Alexandra Woolgar, Bowen Zhou, and Chao Zhang. Brainomni: A brain foundation model for unified eeg and meg signals. In *The Thirty-ninth Annual Conference on Neural Information Processing Systems*, 2025.

Qizhe Xie, Minh-Thang Luong, Eduard Hovy, and Quoc V Le. Self-training with noisy student improves imagenet classification. In *Proceedings of the IEEE/CVF conference on computer vision and pattern recognition*, pages 10687–10698, 2020.

Yucheng Xing, Ling Huang, Jingying Ma, Ruping Hong, Jiangdong Qiu, Pei Liu, Kai He, Huazhu Fu, and Mengling Feng. Dpsurv: Dual-prototype evidential fusion for uncertainty-aware and interpretable whole-slide image survival prediction. *arXiv preprint arXiv:2510.00053*, 2025.

I Zeki Yalniz, Hervé Jégou, Kan Chen, Manohar Paluri, and Dhruv Mahajan. Billion-scale semi-supervised learning for image classification. *arXiv preprint arXiv:1905.00546*, 2019.

Chaoqi Yang, M Westover, and Jimeng Sun. Biot: Biosignal transformer for cross-data learning in the wild. *Advances in Neural Information Processing Systems*, 36:78240–78260, 2023.

Shihao Yang, Xiyi Huang, Danilo Bernardo, Jun-En Ding, Andrew Michael, Jingmei Yang, Patrick Kwan, Ashish Raj, and Feng Liu. Foundation and large-scale ai models in neuroscience: A comprehensive review. *arXiv preprint arXiv:2510.16658*, 2025.

Elissa Ye, Haoqi Sun, Michael J Leone, Luis Paixao, Robert J Thomas, Alice D Lam, and M Brandon Westover. Association of sleep electroencephalography-based brain age index with dementia. *JAMA network open*, 3(9):e2017357–e2017357, 2020.

Zhizhang Yuan, Fanqi Shen, Meng Li, Yuguo Yu, Chenhao Tan, and Yang Yang. Brainwave: A brain signal foundation model for clinical applications. *arXiv preprint arXiv:2402.10251*, 2024.

Bowen Zhang, Yidong Wang, Wenxin Hou, Hao Wu, Jindong Wang, Manabu Okumura, and Takahiro Shinozaki. Flexmatch: boosting semi-supervised learning with curriculum pseudo labeling. In *Proceedings of the 35th International Conference on Neural Information Processing Systems*, pages 18408–18419, 2021a.

Daoze Zhang, Zhizhang Yuan, Junru Chen, Kerui Chen, and Yang Yang. Brant-x: A unified physiological signal alignment framework. In *Proceedings of the 30th ACM SIGKDD Conference on Knowledge Discovery and Data Mining*, pages 4155–4166, 2024.

Pan Zhang, Bo Zhang, Ting Zhang, Dong Chen, Yong Wang, and Fang Wen. Prototypical pseudo label denoising and target structure learning for domain adaptive semantic segmentation. In *Proceedings of the IEEE/CVF conference on computer vision and pattern recognition*, pages 12414–12424, 2021b.

Ping Zhang, Zheda Mai, Quang-Huy Nguyen, and Wei-Lun Chao. Revisiting semi-supervised learning in the era of foundation models. *arXiv preprint arXiv:2503.09707*, 2025.

Qingru Zhang, Minshuo Chen, Alexander Bukharin, Pengcheng He, Yu Cheng, Weizhu Chen, and Tuo Zhao. Adaptive budget allocation for parameter-efficient fine-tuning. In *International Conference on Learning Representations*. Openreview, 2023.

Xiao Zhang and Ji Wu. Dissecting learning and forgetting in language model finetuning. In *The Twelfth International Conference on Learning Representations*, 2024.

Wei-Long Zheng and Bao-Liang Lu. Investigating critical frequency bands and channels for eeg-based emotion recognition with deep neural networks. *IEEE Transactions on autonomous mental development*, 7(3):162–175, 2015.

Huihui Zhou, Aiping Liu, Shizhen Ding, Jing Yao, and Xun Chen. An interpretable single-channel eeg sleep staging model based on prototype matching and multi-task learning. *IEEE Sensors Journal*, 2024.

Songchi Zhou, Ge Song, Haoqi Sun, Deyun Zhang, Yue Leng, M Brandon Westover, and Shenda Hong. Continuous sleep depth index annotation with deep learning yields novel digital biomarkers for sleep health. *npj Digital Medicine*, 8(1):203, 2025a.

Xinliang Zhou, Chenyu Liu, Zhisheng Chen, Kun Wang, Yi Ding, Ziyu Jia, and Qingsong Wen. Brain foundation models: A survey on advancements in neural signal processing and brain discovery. *arXiv preprint arXiv:2503.00580*, 2025b.

Yuchen Zhou, Jiamin Wu, Zichen Ren, Zhouheng Yao, Weiheng Lu, Kunyu Peng, Qihao Zheng, Chunfeng Song, Wanli Ouyang, and Chao Gou. Csbrain: A cross-scale spatiotemporal brain foundation model for eeg decoding. *arXiv preprint arXiv:2506.23075*, 2025c.

Xiaojin Jerry Zhu. Semi-supervised learning literature survey. 2005.

Igor Zyma, Sergii Tukaev, Ivan Seleznov, Ken Kiyono, Anton Popov, Mariia Chernykh, and Oleksii Shpenkov. Electroencephalograms during mental arithmetic task performance. *Data*, 4(1):14, 2019.

## A Theoretical Analysis

### A.1 Proof of Proposition 3.1

**Proposition 3.1.** Let  $\{\tilde{\mathbf{w}}_k\}_{k=1}^K \subset \mathbb{S}^{d-1}$  be the normalized classifier weights. If they satisfy the simplex equiangular tight frame condition  $\tilde{\mathbf{w}}_k^\top \tilde{\mathbf{w}}_{k'} = -\frac{1}{K-1}$ ,  $\forall k \neq k'$ , the minimum pairwise angular separation is maximized.

*Proof.* Since the cosine function is monotonically decreasing on  $[0, \pi]$ , this is equivalent to minimizing the maximum pairwise cosine similarity, defined as  $\eta_{\max} = \max_{k \neq k'} \tilde{\mathbf{w}}_k^\top \tilde{\mathbf{w}}_{k'}$ .

Consider the squared Euclidean norm of the sum of these vectors. By the non-negativity of the norm, we have:

$$\left\| \sum_{k=1}^K \tilde{\mathbf{w}}_k \right\|^2 = \sum_{k=1}^K \|\tilde{\mathbf{w}}_k\|^2 + \sum_{k \neq k'} \tilde{\mathbf{w}}_k^\top \tilde{\mathbf{w}}_{k'} \geq 0. \quad (15)$$

Since  $\|\tilde{\mathbf{w}}_k\| = 1$  for all  $k$ , the first term sums to  $K$ .

$$K + \sum_{k \neq k'} \tilde{\mathbf{w}}_k^\top \tilde{\mathbf{w}}_{k'} \geq 0 \quad (16)$$

Then:

$$\sum_{k \neq k'} \tilde{\mathbf{w}}_k^\top \tilde{\mathbf{w}}_{k'} \geq -K \quad (17)$$

For the second term, in the summation  $\sum_{k \neq k'} \tilde{\mathbf{w}}_k^\top \tilde{\mathbf{w}}_{k'}$ , there are  $K(K-1)$  terms (i.e., all off-diagonal elements). we can bound the sum using  $\rho_{\max}$ :

$$\sum_{k \neq k'} \tilde{\mathbf{w}}_k^\top \tilde{\mathbf{w}}_{k'} \leq \sum_{k \neq k'} \eta_{\max} = K(K-1)\eta_{\max}. \quad (18)$$

Substituting this into the expansion of the norm yields:

$$K(K-1)\eta_{\max} \geq K. \quad (19)$$

Divide both sides by  $K(K-1)$ .

$$\eta_{\max} \geq \frac{-K}{K(K-1)} \quad (20)$$

Rearranging the inequality provides a lower bound on the maximum cosine similarity (known as the Rankin bound):

$$\eta_{\max} \geq -\frac{1}{K-1}. \quad (21)$$

For any set of  $K$  unit vectors, the largest cosine similarity among them is at least  $-\frac{1}{K-1}$ .

The proposition states that the vectors satisfy the simplex equiangular tight frame (ETF) condition:  $\tilde{\mathbf{w}}_k^\top \tilde{\mathbf{w}}_{k'} = -\frac{1}{K-1}$  for all  $k \neq k'$ . In this configuration, the pairwise cosine similarity is uniform and exactly equals the theoretical lower bound. Consequently, the maximum cosine similarity is minimized, which implies that the minimum pairwise angular separation is maximized.

### A.2 Proof of Lemma 3.2

**Lemma 3.2.** In the singleton-only scenario and without ignorance mass, the Dempster-Shafer combination rule degenerates to  $m(\{\omega_c\}) = \frac{m_1(\{\omega_c\})m_2(\{\omega_c\})}{\sum_j m_1(\{\omega_j\})m_2(\{\omega_j\})}$ , where  $m_1(\cdot)$  and  $m_2(\cdot)$  denote the basic belief assignments (BBAs) provided by two evidence sources, and  $\omega_c \in \Omega$  represents the  $c$ -th singleton hypothesis in the frame of discernment  $\Omega$ .

*Proof.* Let  $\Omega = \{\omega_1, \dots, \omega_C\}$  denote the frame of discernment. Under the singleton-only assumption, the basic belief assignments (BBAs)  $m_1(\cdot)$  and  $m_2(\cdot)$  allocate mass exclusively to singleton hypotheses, i.e.,  $m_i(A) = 0$  for all  $A \subseteq \Omega$  with  $|A| > 1$ , and no ignorance mass is assigned.

The Dempster-Shafer combination rule for two BBAs is given by

$$m(A) = \frac{1}{1-K} \sum_{B \cap C = A} m_1(B) m_2(C), \quad (22)$$

where the conflict term  $K$  is defined as

$$K = \sum_{B \cap C = \emptyset} m_1(B) m_2(C). \quad (23)$$

For any singleton hypothesis  $\{\omega_c\}$ , the condition  $B \cap C = \{\omega_c\}$  is satisfied if and only if  $B = C = \{\omega_c\}$ . Therefore, the numerator reduces to

$$\sum_{B \cap C = \{\omega_c\}} m_1(B) m_2(C) = m_1(\{\omega_c\}) m_2(\{\omega_c\}). \quad (24)$$

Moreover, since all mass is assigned to singleton hypotheses, the total non-conflicting mass is

$$1 - K = \sum_{j=1}^C m_1(\{\omega_j\}) m_2(\{\omega_j\}). \quad (25)$$

Substituting the above results into the Dempster-Shafer combination rule yields

$$m(\{\omega_c\}) = \frac{m_1(\{\omega_c\}) m_2(\{\omega_c\})}{\sum_{j=1}^C m_1(\{\omega_j\}) m_2(\{\omega_j\})}, \quad (26)$$

## B Detailed Related work

### B.1 EEG Foundation Models

In this work, we focus on scalp EEG EFM as general-purpose encoders, targeting scalable and non-invasive EEG representation learning. Beyond the rapid development of scalp EEG foundation models, related efforts have explored other derivative forms of EEG. iEEG (intracranial electroencephalography) provides high signal fidelity and spatial resolution. Chen et al. [2022] proposes a method for effectively modeling iEEG signals using Hierarchical Graph Diffusion Learning. Cai et al. [2023] brings a multi-channel self-supervised learning framework for iEEG Signals. Besides, Brant-X [Zhang et al., 2024] and Brainwave [Yuan et al., 2024] attempt to unify the representation of iEEG and other medical time series in deep learning. These models are widely used for the detection of certain diseases, such as seizures [Tu et al., 2024, Shoeibi et al., 2021].

Other efforts explore alternative directions that are Large Language Model (LLM)-centric modeling [Jiang et al., 2025, Lu et al., 2025]. Jiang et al. [2025] regards EEG as a language and uses LLM to model EEG. Lu et al. [2025] brings a new direction, they design a neural-language connector was designed to bridge the modality gap between neural signals and large language models. Neuro-GPT Cui et al. [2024], ECHO Liu et al. [2025], and Uni-NTFM [Chen et al., 2025] improved the common backbone transformer of LLM models to better integrate with the characteristics of EEG data. Self-supervised learning is also one of the improvement directions for these LLM-centric methods. For example, works like BrainOmni [Xiao et al., 2025] and NeurIPT Fang et al. [2025] have improved the coupling methods between EEG and different modalities.

### B.2 Semi-supervised Learning

Semi-supervised learning (SSL) aims to leverage abundant unlabeled data together with limited labeled samples, and has become a promising paradigm for learning under data-scarce settings Zhu [2005], Van Engelen and Hoos [2020]. In the deep learning era, a series of effective SSL methods have been proposed, among which FixMatch Sohn et al. [2020] and MixMatch Berthelot et al. [2019] are representative approaches. These methods typically rely on lightweight backbone models and exploit consistency regularization and pseudo-labeling to achieve strong empirical performance. With the emergence of foundation models, SSL faces new challenges. Foundation models usually contain a large number of parameters, making full fine-tuning computationally expensive Zhang et al. [2025]. To address this issue, parameter-efficient tuning strategies, such as LoRA Hu et al. [2022], have been widely adopted. Despite their strong zero-shot and few-shot capabilities, foundation models remain vulnerable to noisy pseudo-labels in semi-supervised settings, which can significantly degrade downstream performance Yalniz et al. [2019], Xie et al. [2020].

In the EEG domain, semi-supervised learning has been studied for various applications, including emotion recognition, sleep staging, and brain-computer interfaces-related tasks Qiu et al. [2024], Dai et al. [2022], Jiang et al. [2023], Al-Asadi et al. [2024]. However, most existing methods are designed for task-specific or relatively small-scale models Weng et al. [2025]. As research attention gradually shifts toward EEG foundation models (EFMs), the integration of semi-supervised learning with EFM remains largely underexplored.

### B.3 Prototype Learning

Prototype-based metric learning methods, such as Prototypical Networks[Snell et al., 2017], are widely used for few-shot classification by representing each class with a prototype (typically the class centroid) in an embedding space and classifying queries by distance to these prototypes. Prototype learning is widely used in the fields of CV, such as ProDA [Zhang et al., 2021b], it provides information using feature distances from prototypes and is used to estimate the likelihood of pseudo-labels for online correction during training. DPSurv [Xing et al., 2025] uses prototype learning to classify case slices separately. However, there are some difficulties in applying prototype learning in the field of EEG. For example, Tang et al. [2025] proposed further improvements for the interpretability of deep learning models on EEG images. In addition, prototype learning usually requires the assistance of rules to better train on EEG data [Al-Hussaini et al., 2019, Zhou et al., 2024]. Niknazar and Mednick [2024] built an EEG expert system to assist with prototype learning. Overall, prototype-based learning provides a structured way to capture essential class-level information in representation space, offering an intuitive mechanism for relating inputs to semantic targets.

### B.4 Dempster–Shafer theory

Decision making under uncertainty remains a fundamental challenge, as modeling uncertainty and integrating heterogeneous evidence are inherently difficult. Dempster–Shafer (DS) theory [Shafer, 1992] extends probabilistic reasoning by allowing belief to be assigned to sets of hypotheses rather than only singleton outcomes, enabling explicit modeling of uncertainty and evidence conflict. A key component of DS theory, Dempster’s rule of combination, provides a principled framework for aggregating multiple independent sources of evidence.

DS theory was first introduced into neural networks by Denœux [2000], who proposed an adaptive pattern classifier based on the DS theory of evidence. This pioneering work established a connection between evidential reasoning and neural network–based learning, enabling uncertainty-aware decision making beyond probabilistic outputs. Building upon this foundation, DS theory has since been extended to modern deep learning settings and applied to a variety of tasks, including image classification and segmentation [Tong et al., 2021, Huang et al., 2022, 2024a, 2025a], where modeling uncertainty and handling ambiguous predictions are particularly important.

More recently, Dempster–Shafer theory has been extended to regression tasks through the introduction of Gaussian Random Fuzzy Numbers (GRFNs), which enable continuous-valued predictions while explicitly modeling epistemic uncertainty [Denœux, 2023b]. Specifically, Denœux [2023a] proposed a DS-based evidential framework for traditional regression problems, formulating predictions as fuzzy random variables with associated belief structures. Building upon this formulation, Huang et al. [2025b, 2024b, 2025c], Xing et al. [2025] further extended the framework to more complex time-to-event and survival analysis settings, demonstrating the applicability of DS-based regression under censored data and long-term outcome modeling.

## C Dataset Description

For evaluation, we consider three public EEG datasets spanning distinct cognitive and affective paradigms, including sleep staging, emotion recognition, and mental workload assessment. These datasets cover both multi-class and binary classification tasks and exhibit substantial diversity in recording protocols, channel configurations, signal durations, and subject populations, with detailed dataset statistics summarized in Table 3. To ensure a realistic assessment of cross-subject generalization, all datasets are evaluated under strict subject-wise splits, where labeled and unlabeled training subjects, validation subjects, and test subjects are mutually exclusive.

### C.1 Sleep Staging

The subset1 of ISRUC-Sleep dataset [Khalighi et al., 2016] is used for the sleep staging task. It consists of overnight polysomnographic EEG recordings collected from 100 subjects and annotated according to the American Academy of Sleep Medicine (AASM) standard into five sleep stages: Wake, N1, N2, N3, and REM. EEG signals are recorded using six channels and sampled at 200 Hz. Following standard practice, the continuous recordings are segmented into non-overlapping 30-second epochs, with each epoch treated as an individual sample. In this work, we adopt a strict subject-wise split to evaluate cross-subject generalization, where subjects 1–24 are used for labeled training, subjects 25–80 for unlabeled training, subjects 81–90 for validation, and subjects 91–100 for testing. Cohen’s Kappa and weighted F1 score are used as evaluation metrics for this multi-class classification task.

Considering the sequential nature of sleep staging, and following prior work[Wang et al., 2025a, Zhou et al., 2025c, Wang et al., 2025b, Ma et al., 2025c], we formulate the task as a sequence-to-sequence prediction problem.

Specifically, a sequence of 20 consecutive epochs is used as input, and the corresponding sequence of sleep stage labels is predicted. To model temporal dependencies across epochs, an additional Transformer layer is applied before the final classifier. This sequential modeling is implemented using the existing sequence-aware classifier of the EFM. The final classifier is a two-layer MLP, mapping epoch-level representations to the five sleep stages, with dimensions  $30\text{s} \times 200\text{ Hz} \rightarrow 512 \rightarrow 5$ .

## C.2 Emotion Recognition

The SEED dataset [Zheng and Lu, 2015] is employed for EEG-based emotion recognition. It contains EEG recordings from 15 subjects exposed to audiovisual stimuli designed to elicit emotional responses. Original annotations include three emotion categories: Positive, Neutral, and Negative. To align with common baseline settings, we remove samples labeled as Neutral and formulate the task as a binary classification problem between Positive and Negative emotions. EEG signals are recorded using 62 channels and segmented into non-overlapping 4-second windows. For fair evaluation under inter-subject variability, a subject-wise split is adopted, where subjects 1–3 are used for labeled training, subjects 4–10 for unlabeled training, subjects 11–12 for validation, and subjects 13–15 for testing. Model performance is evaluated using AUROC and AUPRC, which are appropriate for binary classification under class imbalance.

The classifier is implemented as a multi-layer perceptron (MLP) that operates on the flattened input representation, with architecture  $60 \times 4 \times 200 \rightarrow 4 \times 200 \rightarrow 200 \rightarrow 1$ . Each hidden layer is followed by an ELU activation and dropout for regularization.

## C.3 Workload Assessment Mental Arithmetic

The Mental Arithmetic dataset [Zyma et al., 2019] supports the task of mental stress detection using EEG signals. It contains recordings from 36 subjects under two distinct cognitive conditions: resting and active engagement in mental arithmetic. EEG data labeled as “no stress” correspond to resting periods prior to the task, while “stress” labels are assigned to recordings during task performance. The signals were acquired using 20 electrodes placed according to the international 10–20 system, with an original sampling rate of 500 Hz. For consistency, the signals are resampled to 200 Hz and band-pass filtered between 0.5–45 Hz to suppress noise. Each recording is segmented into 5-second windows, yielding a total of 1,707 samples. We adopt a subject-wise split for fair evaluation with existing baselines: subjects 1–8 for labeled training, 9–28 for unlabeled training, 29–32 for validation, and 33–36 for testing.

For the this task with 5-second EEG segments sampled at 200 Hz, the classifier is implemented as a multi-layer perceptron (MLP). For backbones that do not use a reference electrode (i.e., CSBrain[Zhou et al., 2025c] and LaBraM[Jiang et al., 2024]), the input consists of 19 channels, and the classifier maps flattened representations of size  $19 \times 5 \times 200 \rightarrow 5 \times 200 \rightarrow 200 \rightarrow 1$ , with GELU activations and dropout applied between layers. For other backbones that retain the reference electrode, 20-channel inputs are used, and the classifier follows the architecture  $20 \times 5 \times 200 \rightarrow 5 \times 200 \rightarrow 200 \rightarrow 1$ , with ELU activations and dropout applied between layers.

Table 3: Dataset Configurations

Dataset	Task	Labeled Training Subjects	Unlabeled Training Subjects	Validation Subjects	Test Subjects	Shape
ISRU	Sleep Staging	1-24	25-80	81-90	91-100	6 ch $\times$ 30s
SEED	Emotion Recognition	1-3	4-10	11-12	13-15	62 ch $\times$ 4s
Mental Arithmetic	Workload Assessment	1-8	9-28	29-32	33-36	20 ch $\times$ 5s

## D Metrics

To comprehensively evaluate our model, we compare it with a set of strong baselines commonly used in EEG analysis. These baselines are evaluated using metrics tailored for class-imbalanced scenarios, which are prevalent in EEG datasets. The metrics include:

**For binary classification:**

**AUROC** and **AUPRC**, which assess the performance of binary classifiers under different thresholds. While AUROC measures the trade-off between sensitivity and specificity, AUPRC focuses on precision-recall trade-offs, especially informative under severe class imbalance.

- For **AUROC**, it measures the model’s ability to distinguish between positive and negative classes by plotting the True Positive Rate (TPR) against the False Positive Rate (FPR) at various thresholds. TPR and FPR can be defined as:

$$TPR = \frac{TP}{TP + FN}, FPR = \frac{FP}{FP + TN}, \quad (27)$$

where TP denotes the number of true positives, TN denotes the number of true negatives, FP denotes the number of false positives, FN denotes the number of false negatives. Then AUROC is defined as:

$$AUROC = \int_0^1 TPR d(FPR), \quad (28)$$

For **AUPRC**, it evaluates the trade-off between precision and recall at different decision thresholds. It is calculated as the area under the curve plotted with precision on the y-axis and recall on the x-axis:

$$AUPRC = \int_0^1 Precision d(Recall), \quad (29)$$

where the  $Precision = \frac{TP}{TP+FP}$  and  $Recall = \frac{TP}{TP+FN}$ .

#### For multi-class classification:

- **Cohen’s Kappa**, which quantifies inter-class agreement beyond chance and is employed as the primary metric for multi-class classification. The Kappa can be calculated by:

$$\kappa = \frac{p_o - p_e}{1 - p_o}, \quad (30)$$

where  $p_o$  denotes the observed agreement and  $p_e$  denotes the expected agreement.

- **Weighted F1 Score**, which combines precision and recall while adjusting for class support, ensuring fair performance measurement across imbalanced datasets.

$$weight\ F1 = \sum_{i=1}^C w_i \frac{2 * Precision * Recall}{Precision + Recall}, \quad (31)$$

where  $w_i$  is the weight of class  $i$ .

## E Baseline and Backbone Models

### E.1 Baseline Models

We evaluate our method under a data-limited adaptation setting, where only a small portion of labeled samples is available. We consider two complementary groups of baselines.

First, we include commonly used lightweight EEG models trained directly on the target datasets under the same limited-supervision condition. These models reflect the performance achievable without leveraging large-scale pretraining.

- **EEGNet** [Lawhern et al., 2018]: A compact Convolutional Neural Network that introduced depthwise and separable convolutions to create an efficient architecture for EEG classification. It is designed to generalize effectively across diverse BCI paradigms, demonstrating robust performance even with limited training data.
- **EEG Conformer** [Song et al., 2022]: A compact Convolutional–Transformer architecture for EEG classification that integrates efficient temporal–spatial convolutional feature extraction with self-attention to capture long-range temporal dependencies. By combining local feature learning with global correlation modeling, it provides a framework that generalizes across different EEG decoding paradigms.

Second, we compare against representative adaptation baselines for pretrained backbones, including (i) parameter-efficient fine-tuning (PEFT) methods and (ii) standard semi-supervised learning (SSL) algorithms. These baselines help disentangle the effect of our task-prior supervision mechanism from (a) generic PEFT strategies for adapting large pretrained models and (b) generic SSL objectives based on pseudo-labeling and consistency regularization.

- **LoRA** [Hu et al., 2022]: A parameter-efficient adaptation method that freezes the pretrained model weights and introduces trainable low-rank decomposition matrices into Transformer layers. This design significantly reduces the number of trainable parameters and computational cost for downstream tasks while enabling effective task-specific adaptation of large pretrained models.
- **FixMatch** [Sohn et al., 2020]: A simple and effective semi-supervised learning approach that combines pseudo-labeling with consistency regularization. It generates pseudo-labels from high-confidence predictions on weakly augmented unlabeled samples and trains the model to predict the same labels under strong data augmentation.
- **FineSSL** [Gan and Wei, 2024]: A semi-supervised learning framework that adapts pretrained foundation models to improve the robustness and effectiveness of SSL methods. It addresses bias-related issues in foundation models through balanced margin softmax and decoupled label smoothing, and can be seamlessly integrated with various fine-tuning strategies and modern SSL algorithms.

## E.2 Backbone Models

As a plug-and-play adapter, our method is architecture-agnostic and can be integrated into a wide range of EFMs without modifying backbone parameters. We therefore select five publicly available EEG foundation models with released pretrained weights as backbones, spanning diverse architectural paradigms (three transformer-based models: **LaBraM**, **CBraMod**, **CSBrain**; and two SSM-style models: **EEGMamba**, **CodeBrain**). We briefly introduce each backbone below.

- **LaBraM** [Jiang et al., 2024]: A scalable Transformer framework for learning general-purpose EEG representations from extensive datasets. It is pretrained on a diverse collection of recordings to capture features that are broadly applicable to downstream BCI tasks, utilizing efficient self-attention and task-specific adapters to facilitate fine-tuning.
- **CBraMod** [Wang et al., 2025a]: An EEG foundation model designed to handle complex dependencies in brain signals. It features a criss-cross Transformer architecture with parallel attention mechanisms that independently model spatial and temporal relationships within the data.
- **CSBrain** [Zhou et al., 2025c]: An EEG foundation model that explicitly models the cross-scale spatiotemporal structure of brain signals. Its backbone alternates between Cross-scale Spatiotemporal Tokenization (CST) and Structured Sparse Attention (SSA) layers. CST aggregates multi-resolution temporal patterns and region-wise spatial features into compact, scale-aware tokens, while SSA captures long-range dependencies across temporal windows and anatomical brain regions through structured and sparse attention.
- **EEGMamba** [Wang et al., 2025b]: An EEG foundation backbone built upon state space models to handle long EEG sequences and heterogeneous tasks. It integrates a Spatio-Temporal-Adaptive (ST-Adaptive) module to unify inputs with varying channel numbers and signal lengths, followed by bidirectional Mamba blocks for linear-time global temporal modeling. To support multi-task EEG decoding, EEGMamba further incorporates a task-aware Mixture of Experts (MoE) with a universal expert, enabling both task-specific specialization and shared representation learning across EEG tasks.
- **CodeBrain** [Ma et al., 2025c]: An efficient two-stage EEG foundation model. It first employs a novel TFDual-Tokenizer to generate discrete representations by independently processing temporal and frequency components. Subsequently, its EEGSSM architecture, which integrates structured global convolutions with a sliding window attention mechanism, is trained via masked prediction to efficiently capture the multi-scale dependencies inherent in brain signals.

## F Additional Ablation Studies on Design Choices

To validate our design choices, we present additional ablation results using two representative EEG foundation models on the representative ISRUC dataset: CSBrain [Zhou et al., 2025c], a Transformer-based backbone, and CodeBrain [Ma et al., 2025c], which adopts a structured state-space modeling (SSSM) paradigm. Together, they reflect two dominant modeling families in current EEG foundation model research. These results demonstrate that our method is largely model-agnostic rather than tailored to a specific backbone.

## F.1 Ablation Study on ProAdapter Depth $L$

We explore the impact of *ProAdapter* depth, defined as the number of backbone layers augmented with adapter modules, while keeping all other settings fixed. For both CSBrain (12-layer Transformer) and CodeBrain (8-layer SSSM), ProAdapters are inserted in a *top-down* manner, i.e., starting from the highest layers and progressively extending toward lower layers.

Table 4, Table 5, and Figure 6 show the results of Across both backbones, we observe a clear U-shaped performance trend with respect to adapter depth. When only a small number of layers are adapted, the model lacks sufficient capacity to internalize task-specific structure, resulting in underfitting. Conversely, equipping too many layers with adapters leads to degraded performance, as excessive parameter updates begin to resemble full fine-tuning, allowing noisy supervision to propagate broadly and weakening the constraint imposed by the frozen backbone.

The top-down insertion strategy is motivated by the hierarchical nature of EEG foundation models: higher layers encode more abstract, task-relevant representations, making them more suitable for feature-wise modulation, while lower layers primarily capture generic signal characteristics that should remain stable under limited supervision.

Importantly, adapter depth also introduces a practical trade-off between accuracy and efficiency. Deeper adapters incur higher computational and parameter overhead without proportional performance gains. Based on this trade-off, we adopt a depth of three *ProAdapter* layers in all experiments, which consistently achieves strong performance while preserving the efficiency advantages of parameter-efficient adaptation.

Table 4: Ablation study on *ProAdapter* depths using **CSBrain** (12-layer Transformer backbone).

<i>ProAdapter Depth</i>	Kappa ( $\uparrow$ )	Weighted-F1 ( $\uparrow$ )	Backward FLOPs (G)
0	56.27 $\pm$ 1.49	64.98 $\pm$ 1.16	1.58
1	58.42 $\pm$ 0.69	66.77 $\pm$ 0.92	2.77
2	59.23 $\pm$ 0.70	67.23 $\pm$ 0.75	2.79
3	<b>61.51 <math>\pm</math> 0.55</b>	<b>69.86 <math>\pm</math> 0.69</b>	2.81
4	61.07 $\pm$ 0.63	69.39 $\pm$ 0.54	2.83
5	60.73 $\pm$ 2.44	70.01 $\pm$ 3.38	2.85
6	60.91 $\pm$ 2.09	69.43 $\pm$ 2.42	2.87
7	59.28 $\pm$ 0.90	67.14 $\pm$ 0.94	2.90
8	56.22 $\pm$ 5.16	63.08 $\pm$ 5.84	2.92
9	53.04 $\pm$ 2.97	61.31 $\pm$ 3.50	2.94
10	50.13 $\pm$ 3.30	57.08 $\pm$ 6.30	2.96
11	44.44 $\pm$ 3.37	53.83 $\pm$ 5.48	2.98
12	38.63 $\pm$ 10.56	50.32 $\pm$ 9.92	3.00

Table 5: Ablation study on *ProAdapter* depths using **CodeBrain** (8-layer SSSM backbone).

<i>ProAdapter Depth</i>	Kappa ( $\uparrow$ )	Weighted-F1 ( $\uparrow$ )	Backward FLOPs (G)
0	52.54 $\pm$ 1.40	61.75 $\pm$ 1.25	1.58
1	55.51 $\pm$ 1.72	64.20 $\pm$ 1.76	2.08
2	59.02 $\pm$ 1.46	67.35 $\pm$ 1.08	3.90
3	<b>63.46 <math>\pm</math> 0.98</b>	<b>71.11 <math>\pm</math> 0.74</b>	5.71
4	61.57 $\pm$ 1.27	71.29 $\pm$ 1.56	7.52
5	63.02 $\pm$ 0.96	70.05 $\pm$ 1.11	9.33
6	63.23 $\pm$ 1.56	<b>71.65 <math>\pm</math> 2.12</b>	11.15
7	63.41 $\pm$ 2.45	70.33 $\pm$ 3.30	12.96
8	62.63 $\pm$ 2.43	69.43 $\pm$ 1.14	13.83

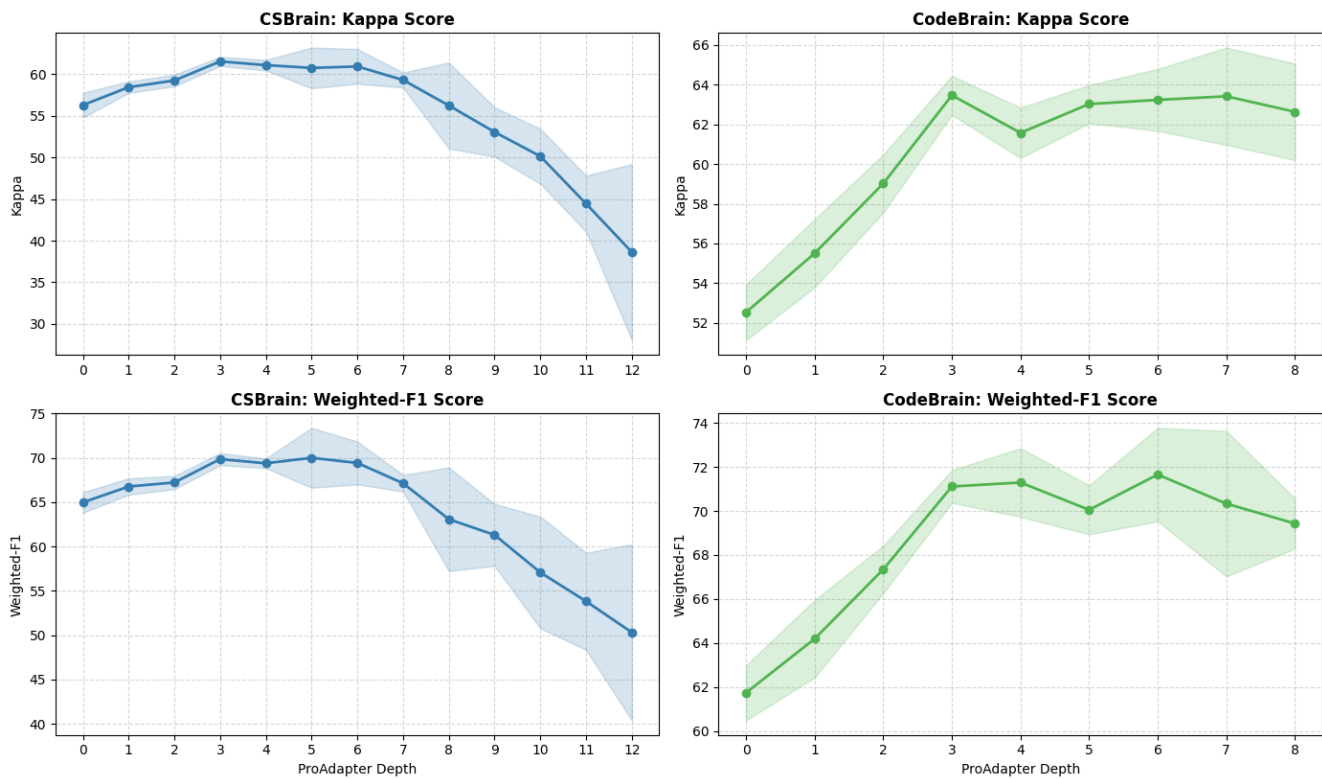


Figure 6: Ablation study on ProAdapter depths

## F.2 Ablation Study on Confidence Threshold $\rho$

We conduct an ablation study on the confidence threshold used for pseudo-label selection in confidence-aware fusion. The threshold  $\rho$  is swept from 0 to 0.95 with a step size of 0.05, where only pseudo-labels whose confidence exceeds the threshold are retained for training.

As shown in Table 6 and Figure 7, model performance exhibits a non-monotonic trend with respect to the confidence threshold. The confidence weighting is important for EEG data because it shows high inter-subject variability, under which a single supervision source, even expert annotation [Jing et al., 2020], can produce supervision with highly heterogeneous reliability across samples. Incorporating unreliable supervision can misdirect optimization [Han et al., 2018], while overly confident supervision biases learning toward easy cases, limiting exposure to informative but ambiguous samples and impairing generalization [Wu et al., 2022, Jain et al., 2024, Sanyal et al., 2025]. An intermediate threshold yields the best performance by balancing pseudo-label quantity and reliability. In this regime, the model benefits from additional supervision while avoiding excessive noise, resulting in more stable and consistent improvements across evaluation metrics. This behavior aligns with the design motivation of confidence-aware fusion, which explicitly regulates how unreliable supervision influences adaptation under limited labeled data.

Based on this trade-off, we select a fixed confidence threshold  $\rho = 0.5$  for all experiments, which consistently achieves strong performance across backbones and tasks.

Table 6: Ablation study on confidence threshold for two representative EEG foundation model backbones. We retain pseudo-labeled samples whose confidence is strictly greater than the threshold.

Confidence	CSBrain (Transformer)		CodeBrain (SSSM)	
	Kappa ( $\uparrow$ )	Weighted-F1 ( $\uparrow$ )	Kappa ( $\uparrow$ )	Weighted-F1 ( $\uparrow$ )
0.00	57.74 $\pm$ 3.52	66.54 $\pm$ 3.65	56.24 $\pm$ 3.48	65.78 $\pm$ 4.03
0.05	59.46 $\pm$ 2.63	67.55 $\pm$ 2.92	58.19 $\pm$ 2.65	66.32 $\pm$ 2.72
0.10	60.03 $\pm$ 1.43	67.96 $\pm$ 1.28	60.23 $\pm$ 1.27	68.71 $\pm$ 1.36
0.15	60.15 $\pm$ 1.23	68.30 $\pm$ 1.29	61.25 $\pm$ 0.98	68.74 $\pm$ 1.26
0.20	60.26 $\pm$ 1.12	68.15 $\pm$ 0.99	61.57 $\pm$ 0.86	68.56 $\pm$ 0.64
0.25	59.78 $\pm$ 1.61	69.08 $\pm$ 1.73	61.88 $\pm$ 1.01	68.87 $\pm$ 0.96
0.30	59.97 $\pm$ 1.13	69.60 $\pm$ 1.72	62.27 $\pm$ 0.72	69.42 $\pm$ 0.95
0.35	60.38 $\pm$ 1.18	69.96 $\pm$ 1.12	62.74 $\pm$ 0.63	71.02 $\pm$ 0.78
0.40	61.27 $\pm$ 0.95	69.01 $\pm$ 0.43	62.73 $\pm$ 1.08	70.85 $\pm$ 1.22
0.45	61.20 $\pm$ 0.68	69.52 $\pm$ 0.70	<b>63.53</b> $\pm$ 1.19	<b>71.31</b> $\pm$ 1.49
0.50	<b>61.51</b> $\pm$ 0.55	<b>69.86</b> $\pm$ 0.69	63.46 $\pm$ 0.98	71.11 $\pm$ 0.74
0.55	<b>61.84</b> $\pm$ 0.43	69.66 $\pm$ 0.52	63.04 $\pm$ 1.43	70.94 $\pm$ 1.57
0.60	61.09 $\pm$ 0.50	69.12 $\pm$ 0.84	62.60 $\pm$ 0.97	70.38 $\pm$ 1.02
0.65	61.72 $\pm$ 0.81	69.50 $\pm$ 0.95	61.89 $\pm$ 1.14	69.46 $\pm$ 1.38
0.70	61.23 $\pm$ 1.05	68.97 $\pm$ 1.24	61.15 $\pm$ 1.82	67.56 $\pm$ 1.71
0.75	60.52 $\pm$ 1.17	68.15 $\pm$ 1.02	59.85 $\pm$ 1.37	66.60 $\pm$ 1.80
0.80	60.53 $\pm$ 1.68	67.94 $\pm$ 1.85	58.98 $\pm$ 1.49	66.62 $\pm$ 1.81
0.85	59.68 $\pm$ 1.95	66.95 $\pm$ 2.55	57.25 $\pm$ 1.85	64.34 $\pm$ 1.76
0.90	57.65 $\pm$ 2.85	65.35 $\pm$ 2.63	56.90 $\pm$ 2.64	64.77 $\pm$ 3.14
0.95	55.93 $\pm$ 3.14	63.76 $\pm$ 3.78	56.33 $\pm$ 2.36	64.25 $\pm$ 2.64

## F.3 Ablation Study on the number of prototypes per class $M$

We investigate the effect of the number of prototypes learned per class,  $M$ , which controls the granularity of class-level structure used in both prototype-based prediction and prototype-conditioned adaptation.

Table 7 and Figure 8 show the result of ablation study on prototype number per class. Using too few prototypes limits the model’s capacity to capture intra-class variability, forcing heterogeneous samples to collapse into a single representative and leading to underfitting. In contrast, an excessive number of prototypes increases structural redundancy and introduces unstable assignments under limited supervision, which may amplify noise in prototype learning and weaken the reliability of prototype-conditioned modulation.

As shown in the following results, an intermediate number of prototypes per class consistently yields the best performance, indicating a favorable balance between expressive class structure and stable optimization. This

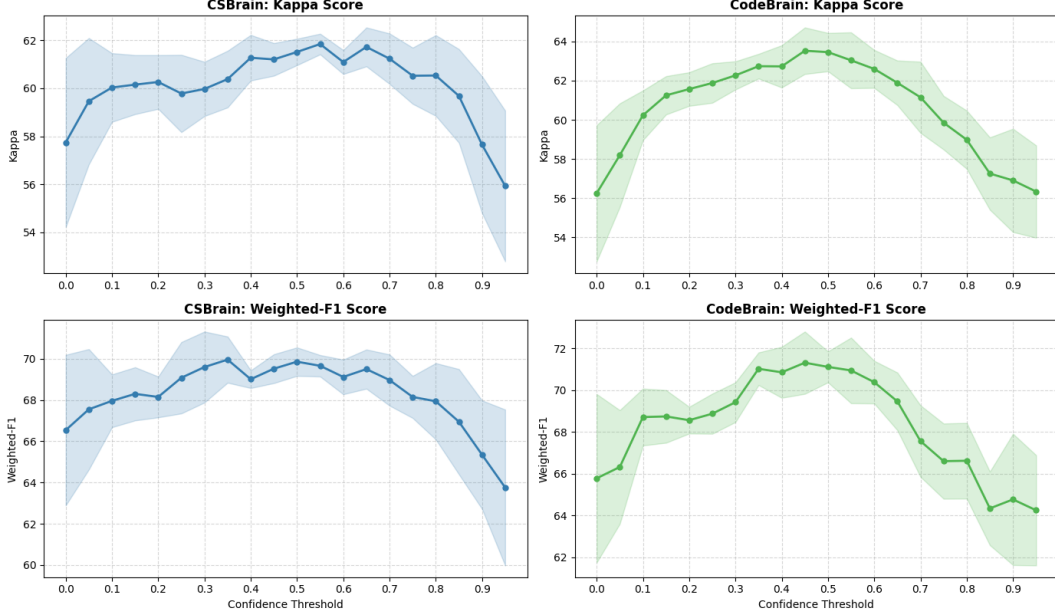


Figure 7: Ablation study on confidence threshold for two representative EEG foundation model backbones.

observation supports the design choice of learning a compact yet diverse set of class prototypes to guide adaptation under label-limited conditions.

Table 7: Ablation study on prototype number per class for two representative EEG foundation model backbones.

Prototype Number per Class	CSBrain (Transformer)		CodeBrain (SSSM)	
	Kappa ( $\uparrow$ )	Weighted-F1 ( $\uparrow$ )	Kappa ( $\uparrow$ )	Weighted-F1 ( $\uparrow$ )
1	$60.38 \pm 0.44$	$68.60 \pm 0.77$	$60.35 \pm 0.81$	$67.95 \pm 0.76$
2	$60.08 \pm 1.21$	$68.08 \pm 1.30$	$62.44 \pm 1.15$	$69.99 \pm 1.79$
3	$61.51 \pm 0.55$	$69.86 \pm 0.69$	$63.46 \pm 0.98$	$71.11 \pm 0.74$
4	$56.89 \pm 1.00$	$65.77 \pm 1.33$	$57.02 \pm 1.09$	$66.01 \pm 1.12$
5	$59.72 \pm 2.61$	$66.64 \pm 3.42$	$60.17 \pm 2.69$	$68.49 \pm 2.83$

#### F.4 Ablation Study on ETF Loss Weights $\lambda_{\text{ETF}}$

We ablate the weight of the Equiangular Tight Frame (ETF) loss applied in the task-prior network (TPN), which regulates the strength of geometric class separation during supervised training. The ETF loss weight  $\lambda_{\text{ETF}}$  is varied over  $\{0.01, 0.05, 0.1, 0.2, 0.5\}$ , while all other components remain unchanged.

As the Table 8 and Figure 9 show, when  $\lambda_{\text{ETF}}$  is too small, the induced class geometry is weak, providing limited structural guidance for subsequent prototype learning and confidence estimation. Conversely, overly large  $\lambda_{\text{ETF}}$  values dominate the optimization objective, constraining the classifier excessively and impairing its ability to fit task-specific variations under limited supervision.

As shown in the results, an intermediate value of  $\lambda_{\text{ETF}} = 0.1$  consistently achieves the best trade-off between geometric regularization and task fitting, and is therefore adopted in all experiments.

#### F.5 Ablation Study on Pesudo-labeled Data Ratio

We study the effect of the pseudo-labeled data ratio, which controls the relative exposure of the model to pseudo-labeled samples during training. Specifically, this ratio determines how many pseudo-labeled samples are introduced after each batch of labeled data, while keeping the batch size fixed at 64 throughout all experiments. Figure 9 shows the results of ablation study on the pseudo-labeled data ratio. For example, a ratio of 0.5 corresponds to 32 pseudo-labeled samples following one labeled batch. This design enforces a controlled balance between reliable

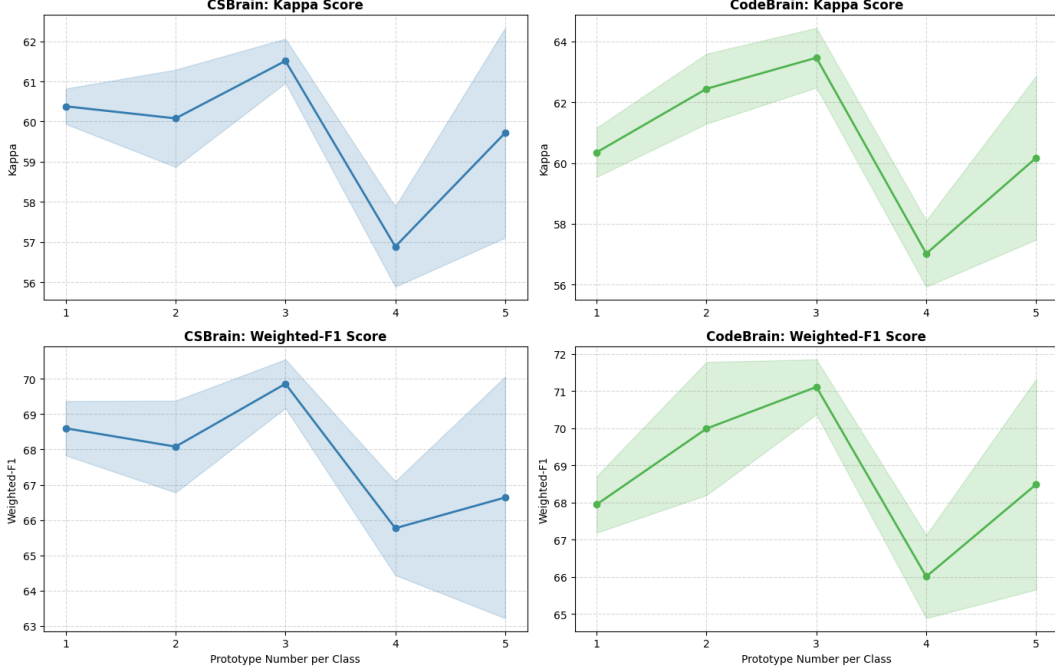


Figure 8: Ablation study on prototype number per class

Table 8: Ablation study on ETF Loss Weights for two representative EEG foundation model backbones.

ETF Loss Weights ( $\lambda_{\text{ETF}}$ )	CSBrain (Transformer)		CodeBrain (SSSM)	
	Kappa ( $\uparrow$ )	Weighted-F1 ( $\uparrow$ )	Kappa ( $\uparrow$ )	Weighted-F1 ( $\uparrow$ )
0.01	59.68 $\pm$ 0.81	66.85 $\pm$ 0.74	60.07 $\pm$ 1.71	66.08 $\pm$ 1.49
0.05	61.44 $\pm$ 1.15	68.99 $\pm$ 1.37	62.77 $\pm$ 1.23	70.93 $\pm$ 1.45
0.1	<b>61.51</b> $\pm$ 0.55	<b>69.86</b> $\pm$ 0.69	<b>63.46</b> $\pm$ 0.98	<b>71.11</b> $\pm$ 0.74
0.2	58.56 $\pm$ 1.45	65.65 $\pm$ 1.59	58.43 $\pm$ 1.18	65.81 $\pm$ 1.64
0.5	54.63 $\pm$ 3.59	62.55 $\pm$ 3.16	54.91 $\pm$ 2.39	63.21 $\pm$ 3.07

supervision from labeled data and additional signals from pseudo-labeled data. When the pseudo-labeled ratio is too high, noisy pseudo-labels may dominate the optimization process, causing the model to drift away from the true task objective. Conversely, an overly small ratio underutilizes unlabeled data and limits the benefit of confidence-aware pseudo-labeling.

By fixing the batch size and varying only the pseudo-labeled ratio, we ensure that each labeled batch serves as a stable anchor that regularly re-aligns the model toward ground-truth supervision. The following ablation results demonstrate that an intermediate ratio yields the best trade-off between leveraging unlabeled data and preserving stable, label-driven adaptation.

Table 9: Ablation study on pesudo-labeled data ratio for two representative EEG foundation model backbones.

Pesudo-labeled Data Ratio	CSBrain (Transformer)		CodeBrain (SSSM)	
	Kappa ( $\uparrow$ )	Weighted-F1 ( $\uparrow$ )	Kappa ( $\uparrow$ )	Weighted-F1 ( $\uparrow$ )
0.5	59.18 $\pm$ 0.55	66.64 $\pm$ 0.83	58.15 $\pm$ 0.64	66.68 $\pm$ 0.51
1	60.24 $\pm$ 0.82	67.88 $\pm$ 0.75	60.68 $\pm$ 1.08	68.40 $\pm$ 1.89
1.5	61.28 $\pm$ 0.79	<b>70.36</b> $\pm$ 1.22	62.24 $\pm$ 1.14	70.45 $\pm$ 1.24
2	<b>61.51</b> $\pm$ 0.55	69.86 $\pm$ 0.69	<b>63.46</b> $\pm$ 0.98	71.11 $\pm$ 0.74
2.5	61.18 $\pm$ 0.73	68.27 $\pm$ 0.99	63.41 $\pm$ 1.67	<b>71.34</b> $\pm$ 1.71
3	60.41 $\pm$ 1.82	67.63 $\pm$ 2.54	63.09 $\pm$ 2.12	70.28 $\pm$ 2.85

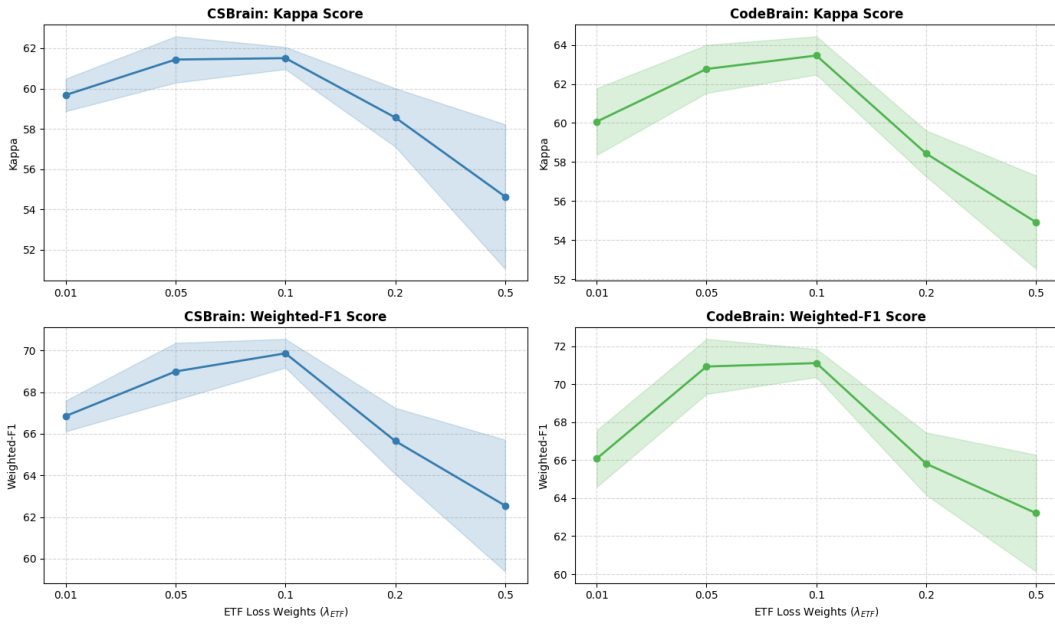


Figure 9: Ablation study on ETF Loss Weights.

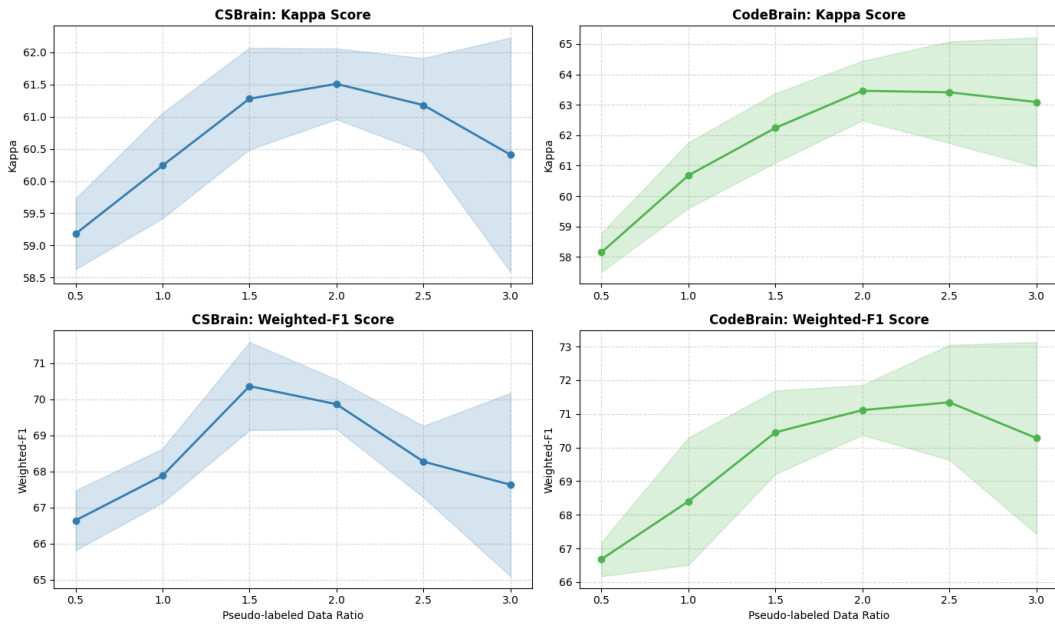


Figure 10: Ablation Study on Pesudo-labeled Data Ratio.

## G Efficiency Analysis

We provide a detailed breakdown of trainable parameters, Backward FLOPs, training time per epoch, and GPU memory usage across all semi-supervised learning and adapter methods. Figure 11 and Table 10 show the information about the baseline and our models under a batch size of 16. Compared to LoRA, which is also an adaptation method, our model shows little difference in trainable parameters and FLOPs. The backward FLOPs of LoRA are higher on Codebrain because Codebrain has more linear layers and convolutional layers in its computational architecture, resulting in greater computational complexity. In contrast, CSBrain has fewer parameters and a simpler model architecture, making the computational complexity of LoRA lower than ours in this case. Since FixMatch performs full parameter fine-tuning, the computational complexity is higher than that of the baselines. Additionally, due to the use of contrastive learning, multiple calculations on augmented samples are required in one epoch, causing Fixmatch to have higher backward FLOPs, GPU memory usage, and training time per epoch compared to full finetuning. These semi-supervised learning methods all have higher computational overhead.

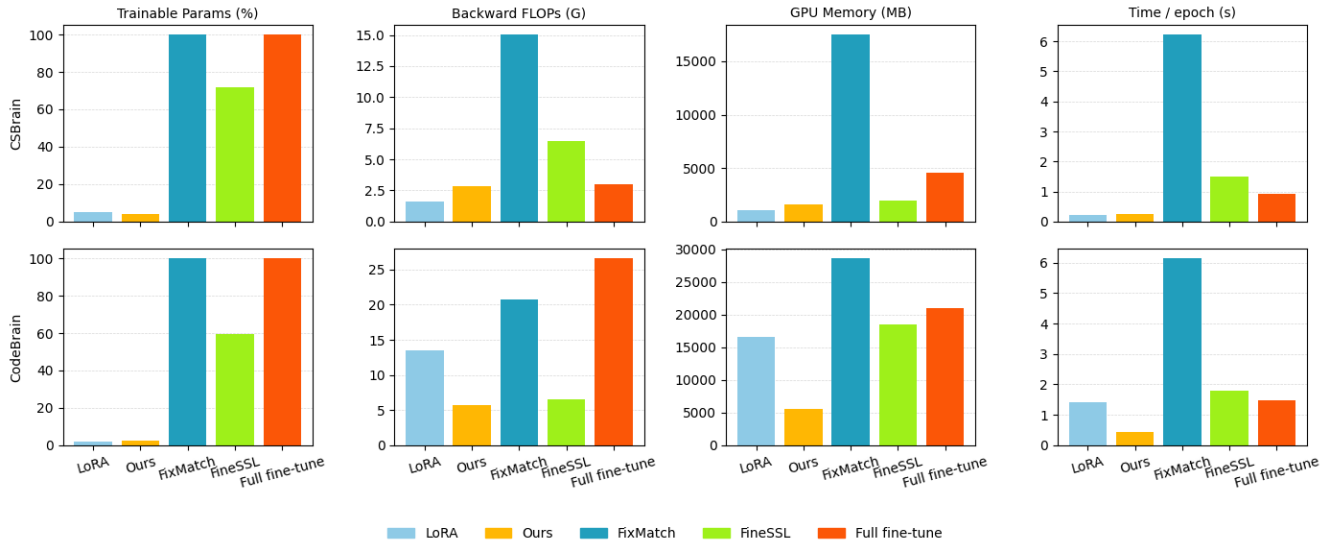


Figure 11: Comparisons of efficiency metric between different baseline model

Table 10: Computational cost comparison on the ISRUC dataset.

Backbone	Method	Params	FLOPs	Mem (MB)	Time
CSBrain	LoRA	5.00%	1.58G	1,034	0.21
	Ours	4.21%	2.81G	1,622	0.26
	FixMatch	100%	15.04G	17,503	6.23
	FineSSL	71.58%	6.50G	1,988	1.51
	Full Fine-tune	100%	2.96G	4,583	0.92
CodeBrain	LoRA	1.91%	13.46G	16,660	1.41
	Ours	2.50%	5.70G	5,530	0.43
	FixMatch	100%	20.76G	28,643	6.15
	FineSSL	59.54%	6.50G	18,512	1.80
	Full Fine-tune	100%	26.60G	21,020	1.49

We further visualize the trade-off between performance and computational efficiency, taking weighted-F1 as an example. In the Figure 12, the horizontal axis denotes training time per epoch (lower is faster), and the vertical axis denotes weighted-F1 score (higher is better). The bubble size indicates GPU memory consumption. Overall, methods located closer to the upper-left corner with smaller bubbles achieve a more favorable balance between performance and efficiency.

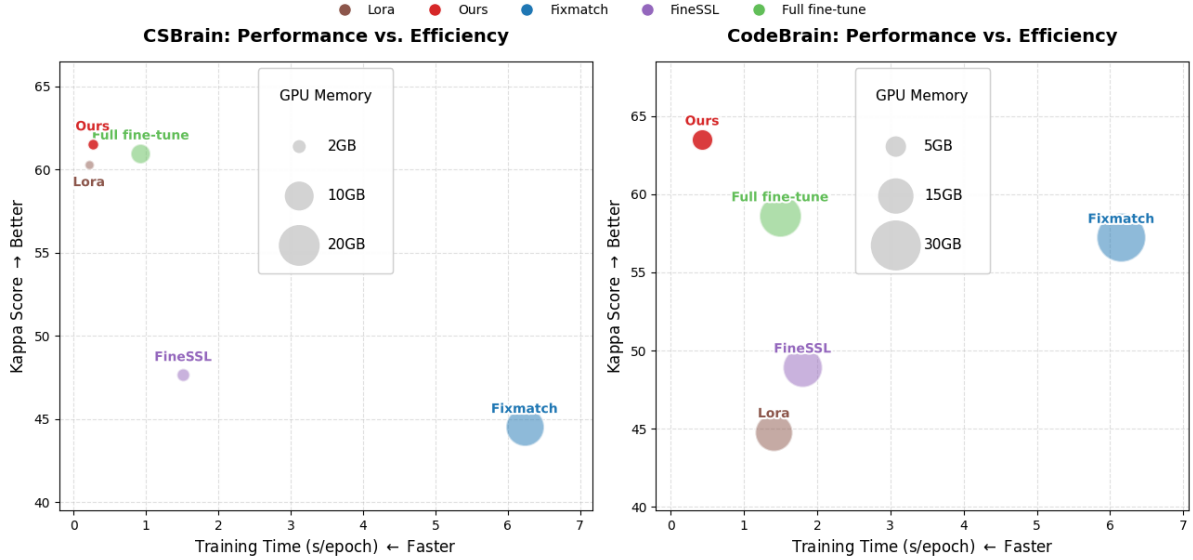


Figure 12: Comparison of computational efficiency of different methods. The method in the figure uses the batch size of 16.

## H Pseudo-Label Quality Analysis

### H.1 With Sinkhorn Constraint

We analyze the quality of pseudo-labels on the ISRUC dataset, which is a multi-class and highly imbalanced EEG benchmark. To provide a comprehensive assessment under class imbalance, we report balanced accuracy (BAcc), Cohen’s Kappa, and weighted F1 score. These metrics together characterize both per-class discrimination and overall agreement, making them well suited for evaluating pseudo-label reliability in this setting. Table 11 shows the pseudo-label quality under confidence-based filtering on the ISRUC dataset, and Figure 14 shows the detailed confusion matrix under different confidence levels in the table. As  $\rho$  increases, the number of agreement samples between TPN and the prototype decreases. Conversely, the kappa and weighted-F1 of their agreement samples improve. In other words, while increasing confidence results in high-quality pseudo-labels, their quantity diminishes. Reviewing the F1 results for different sleep classifications shows that as  $\rho$  increases, both models perform better in classifying Wake and N3 states, whereas classification results for N1 and N2 show a declining trend. The REM state remains largely unchanged with variations in  $\rho$ , indicating that under higher confidence conditions, the model tends to produce results for more prevalent types.

Table 11: Pseudo-label quality under confidence-based filtering on ISRUC. For a threshold  $\rho$ , we retain pseudo-labeled samples with confidence  $\geq \rho$ . We report coverage and pseudo-label quality in terms of Cohen’s Kappa, weighted F1, and per-class F1.

$\rho$	Coverage (%)	Per-class F1						
		Kappa	Weighted-F1	Wake	N1	N2	N3	REM
0.00	72.66	62.49	70.67	87.01	41.57	69.68	78.27	53.93
0.05	72.62	62.50	70.68	87.04	41.54	69.68	78.29	53.93
0.10	72.47	62.59	70.76	87.12	41.51	69.76	78.37	53.90
0.15	72.02	62.78	70.93	87.22	41.42	69.91	78.48	53.96
0.20	70.75	63.32	71.42	87.57	41.07	70.31	78.68	54.13
0.25	68.57	64.15	72.18	88.10	39.50	71.00	78.92	54.64
0.30	65.26	65.28	73.21	88.76	37.46	71.83	79.18	54.91
0.35	61.06	67.02	74.76	89.52	36.06	73.02	79.72	55.68
0.40	56.53	68.84	76.36	90.35	34.10	74.09	80.59	55.91
0.45	51.97	70.56	77.85	91.28	31.35	74.54	81.69	56.62
0.50	47.24	72.15	79.25	92.20	29.66	74.36	83.12	55.66
0.55	42.09	74.42	81.08	93.15	26.43	74.68	85.11	56.28
0.60	37.34	76.47	82.84	93.95	24.31	74.60	87.12	55.84
0.65	33.36	78.12	84.30	94.62	20.57	73.66	88.89	55.81
0.70	29.68	79.65	85.70	95.28	17.03	72.14	90.34	55.47
0.75	26.12	81.16	87.03	95.69	13.76	70.45	91.95	54.37
0.80	22.80	82.93	88.51	96.21	10.63	68.34	93.60	53.81
0.85	19.35	84.84	90.09	96.70	5.94	64.55	95.20	53.38
0.90	15.56	86.09	91.11	97.13	5.76	53.23	96.32	52.01
0.95	10.87	88.15	92.46	97.39	2.47	38.80	97.68	53.57

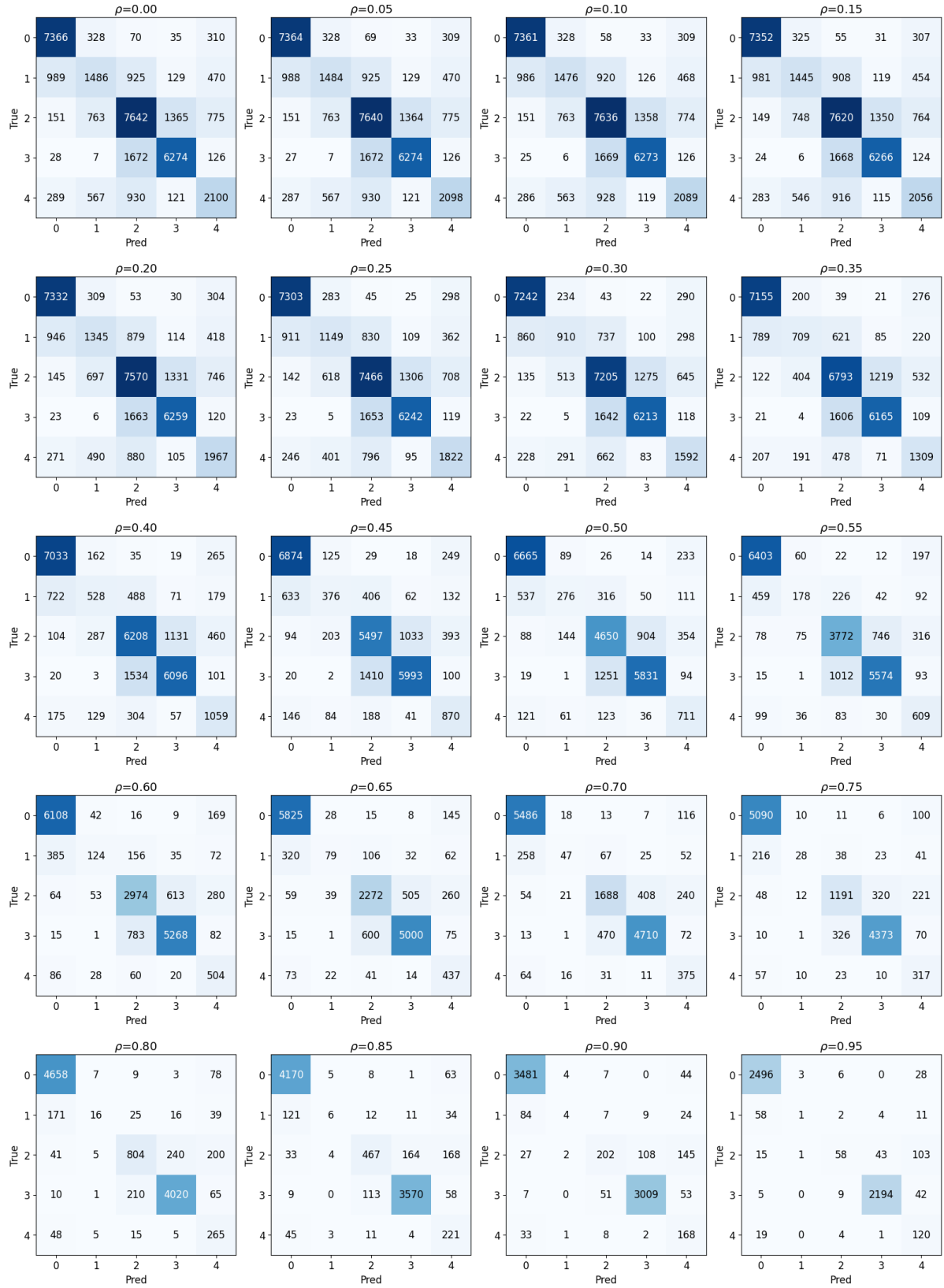


Figure 13: Confusion matrix under different confidence levels.

## H.2 Without Sinkhorn Constraint

For comparison, we also conducted an ablation experiment without the Shikhorn-Knopp algorithm. Table 12 shows the pseudo-label quality under the ablation study of removing Sinkhorn-Knopp algorithm on the ISRUC dataset. Figure 14 shows the detailed confusion matrix under different confidence levels. Compared to the version with the Sinkhorn-Knopp algorithm, the proportion of Coverage is lower at low confidence levels. Although it achieves better overall Kappa and F1 scores, the classification results are extremely poor for N1, as the prototype model hardly predicts any N1s. This label quality introduces new difficulties for subsequent fine-tuning because the model does not encounter enough N1 samples. After incorporating the Sinkhorn-Knopp algorithm, the prototype model can more actively predict rare samples like N1. While this comes at a cost to some accuracy in other categories, due to their larger representation in the dataset, there won't be a situation where categories are missing from pseudo-label datasets. Therefore, this proves that adding constraints in prototype learning can better assist pseudo-label training.

Table 12: Ablation study on removing Sinkhorn–Knopp algorithm on pseudo-label learning. Pseudo-label quality under confidence-based filtering on ISRUC. For a threshold  $\rho$ , we retain pseudo-labeled samples with confidence  $\geq \rho$ .

Per-class F1								
$\rho$	Coverage (%)	Kappa	Weighted-F1	Wake	N1	N2	N3	REM
0.00	55.23	71.70	75.68	89.98	2.09	77.90	85.16	71.13
0.05	55.23	71.70	75.68	89.98	2.09	77.90	85.16	71.13
0.10	55.22	71.71	75.68	89.99	2.10	77.90	85.17	71.11
0.15	55.11	71.78	75.77	90.03	2.11	77.94	85.20	71.18
0.20	54.70	72.04	76.03	90.15	2.16	78.13	85.27	71.32
0.25	53.81	72.47	76.54	90.34	2.28	78.46	85.36	71.42
0.30	52.57	73.11	77.26	90.63	2.46	78.90	85.50	71.64
0.35	50.75	74.02	78.23	91.10	2.37	79.56	85.78	71.82
0.40	48.43	75.05	79.25	91.69	2.53	80.24	86.15	72.08
0.45	46.14	76.10	80.29	92.17	2.70	80.93	86.60	72.24
0.50	43.72	77.19	81.33	92.76	2.72	81.48	87.16	72.50
0.55	41.11	78.43	82.51	93.38	2.94	82.08	87.93	72.28
0.60	38.46	79.57	83.57	93.91	3.16	82.49	88.66	72.46
0.65	35.57	80.82	84.76	94.53	3.21	82.80	89.49	72.27
0.70	32.66	82.03	85.97	95.20	3.64	82.81	90.22	72.05
0.75	29.44	83.55	87.44	95.89	4.29	82.53	91.24	72.91
0.80	26.03	84.61	88.54	96.31	4.90	81.41	92.31	71.79
0.85	22.41	86.19	90.15	96.99	4.86	79.69	93.52	71.73
0.90	18.41	88.08	91.90	97.39	5.95	77.35	95.29	67.78
0.95	13.46	90.75	94.18	98.35	7.79	68.44	96.94	62.91



Figure 14: Confusion matrix at different confidence levels without using the Sinkhorn-Knopp algorithm.

# I Pseudocode for Training Procedure

This section presents the pseudocode of the overall training procedure to facilitate understanding of the workflow. The pseudocode summarizes the key steps involved in external supervision construction, pseudo-label generation, confidence-aware fusion, and parameter update, while omitting implementation-specific details.

---

## Algorithm 1 Training Procedure of SCOPE

---

**Require:** Labeled dataset  $\mathcal{D}_l = \{(X_i, y_i)\}_{i=1}^{N_l}$  with  $y_i \in \{1, \dots, K\}$ ,  $K$  is the number of class;  
1: Unlabeled dataset  $\mathcal{D}_u = \{X_j\}_{j=1}^{N_u}$ ;  
2: Pretrained foundation model parameters  $\theta_{FM}$ ;  
3: Initialized task-prior network (TPN) parameters  $\theta_{TPN}$ ;  
4: Initialized ProAdapter and classifier parameters  $\theta_{PA}, \theta_C$ .  
**Ensure:** Optimized parameters  $\theta_{PA}^*, \theta_C^*$ .

5: **(a) Task Prior Network Training for Inter-class Separability**  
6: Train  $\theta_{TPN}$  on  $\mathcal{D}_l$  using ETF-regularized cross-entropy loss  $\mathcal{L}_{TPN}$ , obtaining  $\theta_{TPN}^*$   
7: Infer prior labels on  $\mathcal{D}_u$ :  $\hat{y}_j^{\text{prior}} \leftarrow \arg \max_c f_{\theta_{TPN}^*}(X_j)_c$   
8: **(b) Prototype-Based Clustering for Intra-class Variability**  
9: Initialize prototype set  $\mathcal{P}$  via  $k$ -means on unlabeled embeddings  $z_j \leftarrow f_{\theta_{TPN}^*}(X_j) \in \mathbb{R}^d$ .  
10: Update  $\mathcal{P}$  by minimizing prototype loss  $\mathcal{L}_P$  on labeled dataset  $\mathcal{D}_l$ .  
11: Derive prototype label  $\hat{y}_j^{\text{proto}} \leftarrow \arg \max_{p \in \mathcal{P}} \text{similarity}(z_j, p)$ .  
12: **(c) Confidence-Aware Fusion (Parameter-Free)**  
13: Obtain the agreement  $\hat{y}_j \leftarrow \mathbb{I}(\hat{y}_j^{\text{prior}} = \hat{y}_j^{\text{proto}})$ .  
14: Obtain reliability scores  $\gamma_j$ .  
15: **(d) ProAdapter Training**  
16:  $\mathcal{L}_{\text{sup}} \leftarrow \frac{1}{|\mathcal{D}_l|} \sum_{(X_j, y_j) \in \mathcal{D}_l} \text{CE}(f_{(\theta_{PA}, \theta_C)}(X_j), y_j)$   
17:  $\mathcal{L}_{\text{pseudo}} \leftarrow \frac{1}{|\mathcal{D}_u|} \sum_{X_j \in \mathcal{D}_u} \text{CE}(f_{(\theta_{PA}, \theta_C)}(X_j), \hat{y}_j)$   
18: Update  $(\theta_{PA}, \theta_C)$  by minimizing  $\mathcal{L}_{\text{sup}} + \gamma_j \cdot \mathcal{L}_{\text{pseudo}}$ .  $\theta_{PA}^*, \theta_C^*$

---

# J HyperParameters Details

## J.1 Details of Task Prior Network (TPN)

TPN is a simple two-block convolutional network, and its specific structure is shown in Table 13. We conducted a grid search over architectural hyperparameters on each dataset to determine the final TPN configuration. Specifically, the labeled set was split into training and validation subsets with an 8:2 ratio, and model selection was performed solely based on validation performance. Importantly, the unlabeled data as well as the validation and test sets used in the main experiments were never accessed during this process. The final TPN architecture we used is shown in Table 14.

## J.2 Details of Prototype learning

We placed the parameters used in the prototype learning section of the paper in Table 15.

## J.3 Fine-tuning Hyperparameters of EFM

Detailed training hyperparameters for EFM are summarized in Tables 16 and 17. Specifically, Table 16 lists the configurations used for fine-tuning on the SEED and Mental Arithmetic datasets, while Table 17 details the settings for the ISRUC dataset.

Table 13: Detailed TPN Architecture and Parameters

Module	Layer / Parameter	Symbol / Default	Output Shape
Input	EEG segment	$(C, T)$	$(1, C, T)$
	Chunk size	$T$	—
	Num electrodes	$C$	—
Block 1	Conv2D	$F_1$ , $\text{kernel}_1$	$(F_1, C, T)$
	BatchNorm2D	—	$(F_1, C, T)$
	DepthwiseConv2D	$D$	$(F_1 \times D, 1, T)$
	BatchNorm2D	—	$(F_1 \times D, 1, T)$
	Activation	ELU	$(F_1 \times D, 1, T)$
	AvgPool2D	$\text{pool}_1$	$(F_1 \times D, 1, T/\text{pool}_1)$
	Dropout	$p$	—
Block 2	SeparableConv2D	$\text{kernel}_2$	$(F_1 \times D, 1, T/\text{pool}_1)$
	Conv2D (1×1)	$F_2$	$(F_2, 1, T/\text{pool}_1)$
	BatchNorm2D	—	$(F_2, 1, T/\text{pool}_1)$
	Activation	ELU	$(F_2, 1, T/\text{pool}_1)$
	AvgPool2D	$\text{pool}_2$	$(F_2, 1, T_{\text{out}})$
	Dropout	$p$	—
Classifier	Linear	$F_2 \times T_{\text{out}} \rightarrow N$	$(N)$
Common Settings	Pooling type	Average	—
	Activation function	ELU	—
	Dropout rate	$p$	—
	Output length	$T_{\text{out}} = \frac{T}{\text{pool}_1 \times \text{pool}_2}$	—

Table 14: Dataset-Specific Hyperparameters settings for TPN

Parameter	ISRUC	MentalArithmetic	SEED
TPN D	2	1	2
TPN $F_1$	16	8	4
TPN $F_2$	32	8	8
TPN dropout	0.1	0.1	0.1
TPN $\text{kernel}_1$	192	256	128
TPN $\text{kernel}_2$	48	32	64
TPN $\text{pool}_1$	8	4	2
TPN $\text{pool}_2$	8	8	4
Linear	248	248	800

Table 15: Configuration of the Prototype Learning

Category	Parameter	Default
Basic Training	Epochs	50
	Batch size	64
	Learning rate	$5 \times 10^{-4}$
	Min learning rate	$1 \times 10^{-6}$
	Weight decay	$5 \times 10^{-3}$
	Optimizer	AdamW
	Optimizer momentum	$\beta_1, \beta_2 = 0.9, 0.999$
	Label smoothing	0.05
	Learning rate schedule	CosineAnnealing
ETF (Equiangular Tight Frame)	ETF $\lambda$	0.1
	ETF scale	10.0
Prototype	Num prototypes per class	3
	Prototype learning rate	0.001
	Init method	KMeans
	Kmeans max per class	5000
	Kmeans $N_{init}$	10
	Prototype $\tau$	10.0
	Prototype temperature	1.0
	Prototype uniform mix	0.05
	Sinkhorn iter	3
Sinkhorn–Knopp	Sinkhorn $\epsilon$	0.05
	Sinkhorn temperature	0.1
	eps	$1 \times 10^{-12}$
Dempster–Shafer Fusion	Confidence threshold $\rho$	0.5

Table 16: Training Hyperparameters of Backbone EFMs on Binary Tasks

Hyperparameter	LaBraM	CBraMod	CSBrain	EEGMamba	CodeBrain
Warm-up Epoch	10	10	10	10	10
Number of Epochs	50	50	50	50	30
Batch Size	64	64	64	16	16
Pseudo Label Batch Size	64	64	64	16	16
Adapter $L$ Layers	3	3	3	3	3
Learning Rate	$1 \times 10^{-5}$	$1 \times 10^{-4}$	$1 \times 10^{-4}$	$1 \times 10^{-4}$	$5 \times 10^{-5}$
Minimum Learning Rate	$1 \times 10^{-6}$				
Weight Decay	0.0001	0.001	0.001	0.001	0.001
Optimizer	AdamW	AdamW	AdamW	AdamW	AdamW
Learning Rate Scheduler	CosineAnnealing	CosineAnnealing	CosineAnnealing	CosineAnnealing	CosineAnnealing
Dropout Rate	0.1	0.1	0.1	0.1	0.1

Table 17: Training Hyperparameters of Backbone EFM<sub>s</sub> on Multi-class Tasks

Hyperparameter	LaBraM	CBraMod	CSBrain	EEGMamba	CodeBrain
Warm-up Epoch	10	10	10	10	10
Number of Epochs	60	60	60	60	60
Batch Size	64	64	64	64	64
Pseudo Label Batch Size	64	64	64	64	64
Adapter $L$ Layers	3	3	3	3	3
Learning Rate	$1 \times 10^{-4}$	$1 \times 10^{-4}$	$1 \times 10^{-4}$	$1 \times 10^{-4}$	$5 \times 10^{-4}$
Minimum Learning Rate	$1 \times 10^{-6}$				
Weight Decay	0.01	0.01	0.01	0.01	0.01
Optimizer	AdamW	AdamW	AdamW	AdamW	AdamW
Learning Rate Scheduler	CosineAnnealing	CosineAnnealing	CosineAnnealing	CosineAnnealing	CosineAnnealing
Dropout Rate	0.1	0.1	0.1	0.1	0.1